

# A scalable adaptive deep Koopman predictive controller for real-time optimization of mixed traffic flow

Hao Lyu, Yanyong Guo, Pan Liu, Nan Zheng, and Ting Wang

**Abstract**—The use of connected automated vehicle (CAV) is advocated to mitigate traffic oscillations in mixed traffic flow consisting of CAVs and human driven vehicles (HDVs). This study proposes an adaptive deep Koopman predictive control framework (AdapKoopPC) for regulating mixed traffic flow. Firstly, a Koopman theory-based adaptive trajectory prediction deep network (AdapKoopnet) is designed for modeling HDVs car-following behavior. AdapKoopnet enables the representation of HDVs behavior by a linear model in a high-dimensional space. Secondly, the model predictive control is employed to smooth the mixed traffic flow, where the combination of the linear dynamic model of CAVs and linear prediction blocks from AdapKoopnet is embedded as the predictive model into the AdapKoopPC. Finally, the predictive performance of the proposed AdapKoopnet is verified using the HighD naturalistic driving dataset. Furthermore, the control performance of AdapKoopPC is validated by the numerical simulations. Results demonstrate that the AdapKoopnet provides more accuracy HDVs predicted trajectories than the baseline nonlinear models. Moreover, the proposed AdapKoopPC exhibits more effective control performance with less computation cost compared with baselines in mitigating traffic oscillations, especially at the low CAVs penetration rates. The code of proposed AdapKoopPC is open source<sup>1</sup>.

**Index Terms**—Mixed traffic flow, Koopman operator theory, Predictive control, Data-driven modeling, Real-time optimization.

## I. INTRODUCTION

WITH the acceleration of urbanization and the increase in the number of motor vehicles, traffic congestion and traffic accidents have become increasingly prominent [1]. Against this background, autonomous driving technology has emerged and is expected to become an innovative solution to alleviate traffic congestion [2], [3]. The most common application is Cooperative Adaptive Cruise Control (CACC), which relies on V2V state sharing to enable vehicles within a vehicle platoon to run at coordinated speeds to maintain a small headway [4]. This technique can enhance traffic capacity

This research was supported by the project of the National Key R&D Program of China (No. 2023YFB4302701), the National Natural Science Foundation of China (No. 51925801, 52232012, 52272343) and Natural Science Foundation of Jiangsu Province (No.BK20221467). (*Corresponding author: Yanyong Guo.*)

Hao Lyu, Yanyong Guo, and Pan Liu are with the School of Transportation, Southeast University, Nanjing 210097, PR China (e-mail: lyu\_hao@seu.edu.cn; guoyanyong@seu.edu.cn; liupan@seu.edu.cn).

Nan Zheng is with the Department of Civil Engineering, Institute of Transport Studies, Monash University, Melbourne, VIC 3800, Australia (e-mail: nan.zheng@monash.edu).

Ting Wang is with the College of Transportation Engineering, Tongji University, Shanghai 201804, PR China (e-mail: 2110763@tongji.edu.cn).

<sup>1</sup><https://github.com/SpaceTrafficSafetyTeam/AdapKoopPC>

and improve safety between vehicles, which has attracted a lot of interest from academia and industry. The excellent performance of connected automated vehicles (CAVs) in a purely intelligent network environment has been widely recognized [5]. In essence, CAV is a mobile scanner that provides historical and real-time trajectory data of individual vehicles [6]. As well, it is also a dynamic actuator for adaptive control [7]. In this intelligent network ideal scenario, vehicles communicate seamlessly and autonomous driving systems operate together accurately and efficiently, thus building a highly intelligent transportation ecosystem [8]. However, the industrialization of autonomous driving technology is a complex process, and the realization of large-scale application of mobile internet and autonomous driving technology is a long process. A more realistic traffic environment is that CAVs and human-driven vehicles (HDVs) share the road. This mixed traffic flow prompts scholars to think deeply and study the performance of CAVs in complex traffic environments [9]. Considering the research topics of this paper, we mainly focus on the following two key points, including the modeling of HDVs behavior and the controlling of CAVs.

**How to model the HDVs driving behavior in dynamic traffic flow, and to predict the HDVs trajectory with high accuracy?** A key goal is to simulate the dynamic driving behaviors of HDVs in mixed traffic flow. These behaviors will be essentially different due to differences in driving environments, drivers, etc. HDV adjusts its own acceleration based on the headway to the leader vehicle, velocity difference, and among others. In term of the physics-driven methods, well-known car-following models were widely employed, such as optimal velocity model [10], full velocity difference model [11], intelligent driver model [12], to describe and model the HDVs behaviors. However, it is known that these time-invariant car-following models always archives high-biased results with large error. With the rapid development of artificial intelligence, big data and computing power, the deep learning methods, including recurrent neural networks (RNN), long short-term memory model (LSTM), deep deterministic policy gradient (DDPG), etc., are being gained more and more interests in modeling the driving behaviors of HDVs. Although deep learning is superior in capturing and modeling driving behavior in complex traffic environments, due to the characteristic of nonlinearity, its shortcomings of slow solution speed and inability to meet real-time optimization control are self-evident.

**How to control CAVs more effectively in mixed traffic**

**flows for mitigating traffic oscillations?** As well known, the jam-absorption driving strategy in the Newell's car-following theory framework was proposed to mitigate the propagation of upstream disturbances, and the corresponding vehicles need to be selected based on the expected absorption speed and real-time traffic conditions to implement the strategy [13]. As mentioned before, CAV is a dynamic executor, and its role is no longer limited to "follower", but has been further expanded to "leader", which is the basic idea and connotation of the Leading Cruise Control (LCC) framework [14]. In addition, the controllability, observability and head-to-tail stability of the LCC framework were also analyzed and verified, confirming its positive role in improving traffic performance [15], [16]. Along this direction, the Data-Enabled Predictive Leading Cruise Control (Deep-LCC) was proposed [17], [18], as an alternative to parametric car-following model, to achieve safe and optimal control of CAVs in mixed platoons. The Deep-LCC has inspired this paper, however, it still exhibits certain limitations. To be specific, in order to use CAVs to positively guide HDVs, it is necessary to first understand the driving behavior changes of HDV after being affected by CAVs. In Deep-LCC, all HDVs follow a rule-based car-following model and add random high-frequency noise to construct the trajectory database. It is obviously unrealistic and limited to combine these trajectories to match the corresponding HDV expected driving trajectories for different scenarios. this is obviously not realistic and has limitations.

Overall, the dilemmas faced by CAV control for traffic optimization in mixed traffic flow lies in accurately modeling and predicting the driving behavior of HDVs in complex scenarios, as well as meeting the requirements of effective and feasible real-time solution and optimization control in reality. Motivated by the above two requirements, the Koopman operator offers a new solution for identifying and analyzing nonlinear systems. The Koopman operator emerges as a highly suitable approach, which facilitates the handling of intricate nonlinear dynamics through linear transformations. This method allows for an efficient modeling of the HDVs behavior without introducing excessive complexity, and its linear properties are well suited for subsequent real-time optimization of mixed traffic flow. Therefore, this paper develops a multi-scenario adaptive deep Koopman predictive control framework for mixed traffic flow. The main contributions of this paper are as follows:

- An adaptive deep Koopman network (AdapKoopnet) is proposed for modeling HDVs car-following behavior with the high-dimensional linear model;
- A scalable state prediction model of mixed traffic flow is developed by integrating linear dynamic model of CAVs and linear prediction blocks from AdapKoopnet;
- An adaptive deep Koopman predictive control framework (AdapKoopPC) based on the state prediction model is proposed for mitigating traffic oscillations in mixed traffic flow.

The framework of this paper is as follows. Section II mainly reviews the relevant literatures and summarizes the research gap. Section III states the AdapKoopnet. Section IV proposes the AdapKoopPC framework. Section V and Section

VI conducts the experiments for HDVs longitudinal trajectory prediction and mixed traffic flow optimization control. At last, the conclusion and prospects are given in Section VII .

## II. RELATED WORK

### A. Driving scenario and characteristics recognition

Recognizing and extracting potential driving scenarios is beneficial for achieving vehicle trajectory prediction with strong generalization ability and accuracy. [19] extracted driving scenarios directly from real driving data and clustered repeated patterns into potential scenario groups without any pre-definition or rules. [20] developed a general active learning framework to annotate driving trajectory time series data and explore unknown driving scenario trajectories. Beyond scenario recognition, more research focuses on capturing driving characteristics. [21] utilized unsupervised algorithms to automatically extract descriptive driving patterns, and the clustered patterns promote a comprehensive understanding of driver behavior characteristics. In addition, identifying the driving style is also a work with practical value. For example, based on the multi-dimensional characteristics, three different driving styles are identified using an unsupervised clustering algorithm [22]. [23] employed a set of experiments to collect driving data among different drivers, and a supervised machine learning-based driving style classifier was designed to recognize the driving style. [24] defined the intermediate variable of neural process as the driving style vector and linked to an interpretable and continuous aggressiveness index. However, identifying and clustering scenarios from natural driving datasets using neural networks without relying on pre-definition or pre-labeling remains to be solved. Secondly, further extracting personalized driving features based on recognized scenarios and using them for driving behavior prediction is also worth exploring.

### B. Car following behavior modeling and trajectory prediction

The trajectory prediction methods of car-following behavior are mainly divided into physics-based methods, data-driven methods, and hybrid-driven methods. The physics-based method uses microscopic traffic flow models for trajectory prediction. For example, [25] explicitly considered the interactions between vehicles and proposed a dynamic Bayesian networks-based filter to estimate the behavior of traffic participants and predict their future trajectories. [26] developed a cooperative intelligent driver model that dynamically determines its acceleration based on parameters such as velocity difference and headway. With the advancement of big data and deep learning technology, data-driven methods for trajectories prediction have been emerging. [27] built spatiotemporal attention long short-term memory (STA-LSTM) for vehicle trajectory prediction, ensuring accuracy while improving interpretability. Pioneeringly, [28] first proposed a physics informed deep learning framework for car-following modeling, taking full advantage of data-driven and physics-based models to surpass existing models. Further, relying on the self-attention mechanism to achieve deeper mining of trajectory features, [29] proposed a Physics-Informed Transformer-Intelligent Driver

Model to predict longitudinal vehicle trajectories. However, there is still a contradiction between the complex deep learning model that describes the nonlinear state evolution of vehicle driving behavior and the requirement that CAV control relies on real-time solutions.

### C. CAV control for optimized mixed traffic flow

Various control approaches have been explored to optimize mixed traffic flow performance such as safety, efficiency and energy consumption. [30] presented a highly efficient platoons control framework based on tube MPC to address heavy computational and communication burden, which mitigates prediction uncertainty through feedback control. [31] implemented a cooperative control strategy for CAVs under the assumption of completely random disturbances triggered by HDVs. Recently, a control strategy called “The Follower Stopper controller” was proposed, and real vehicle experiments demonstrated its ability to improve traffic flow stability [32]. To address the limitation of executing FS policies individually for all CAVs, [33] established a cellular automaton model of mixed traffic flow based on the FS strategy for CAV control, which positively affected the efficiency, oscillation, and fuel consumption of mixed traffic flow. From the perspective of collective function optimization, [34] studied the impact of different formations of CAVs on traffic performance, focusing on the formation of cooperation between CAVs using centralized optimal controllers. Besides, a traffic-smoothing controller was directly learned from trajectories based on a reinforcement learning policy gradient algorithm [35]. [36] integrated an advanced linear controller and a DPPO-based DRL controller to construct a hybrid controller, achieving stable and efficient longitudinal driving of CAVs within mixed flow. [37] developed the robust-safety-critical traffic controller in mixed traffic flow. This controller ensures collision-free safety even in the face of actuator and sensor delays, as well as disturbances from the leading HV. As traffic systems expand, a consequent problem is the dramatic increase in online computing burden, and the data-driven distributed control emerged as the times require. Surprisingly, [38] conducted data-driven mixed vehicle platoons dynamics modeling based on Koopman, which is a groundbreaking work that has attracted our high attention and interest. [17], [18] proposed distributed data-driven predictive control that directly utilizes measurable traffic data to design collision-free optimal CAV control inputs for collaboratively smoothing mixed traffic flows. However, it is difficult to demonstrate its generalization ability in other mixed traffic flow scenarios by modeling the entire traffic flow and obtaining the Koopman operator based on a dataset generated by simple physical models, which drives our idea. We expect to use Koopman theory to learn vehicle features from real-world trajectories and construct a scene adaptive and scalable control framework.

### D. The applications of Koopman theory in traffic flow

Koopman operator theory is a mathematical framework that involves representing nonlinear systems in a higher-dimensional linear space, making it possible to study the evolution of complex systems [39]. [40] used Koopman

operator to propose a model-free, data-driven approach that cleverly analyzed and predicted the evolution of highly complex nonlinear traffic flow. [41] applied Koopman operator theory and the dynamical mode decomposition for signalized traffic flow networks control, which allows for early identification of unstable queue growth. In order to realize the real-time control of the ramp metering on the freeway efficiently, [42] proposed a model predictive controller with the trained deep Koopman model. The above methods relied on parameter estimation of physical models or modeling of nonlinear dynamics using neural networks. [43] introduced a novel data-driven vehicle modeling and control approach, employing an interpretable Koopman operator base deep neural networks in which extended dynamic mode decomposition was utilized to learn a finite-dimensional approximation of the Koopman operator. Recently, in solving non-stationary time series prediction problems, [44] proposed an efficient time series prediction model driven by Koopman theory, which hierarchically mines the dynamic system of time series.

## III. ADAPKOOPNET: ADAPTIVE DEEP KOOPMAN NETWORK FOR CAR FOLLOWING BEHAVIOR MODELING AND PREDICTION OF HDVs

In this section, a data-driven adaptive deep Koopman linear model is proposed to address the challenges associated with real-time cognition and prediction of the state of HDVs.

### A. Key terms definition

Considering that terms such as scenarios have different understandings in existing research. Here we define and explain several key terms that apply specifically to this paper:

*Scenario* is the mixed traffic flow environment in which the vehicle is located, such as free flow, synchronous flow, congestion flow, etc., and the direct explicit status includes traffic flow velocity, density, etc.

*Scenario characteristics* refers to the collective driving behavior exhibited by drivers in corresponding scenes, which is a potential common feature. For example, in high-velocity and high-density driving scenario, drivers generally pay more attention to the behavior of surrounding vehicles, are greatly influenced by them, and adjust their own driving behavior more frequently than usual.

*Driving characteristics* is the specific manifestations of an individual driver’s long-term driving habits in different driving scenarios. For example, aggressive drivers may be more conservative in high-velocity and high-density scenarios compared to free flow scenarios. However, this tendency is uncertain. Some drivers exhibit driving characteristics similar to the average of vehicle group characteristics in certain scenarios, while others are only slightly affected. Therefore, the predicted scenario classification is the comprehensive value of driver tendency and scenario characteristics themselves.

### B. Problem description

Assuming that in high-density mixed traffic flow, HDVs not engaging in lane-changing behavior are primarily influenced by their preceding vehicles. Their driving behavior is primarily

shaped by the current velocity of the preceding vehicle, their own current velocity, and the headway. For the purpose of research, time is discretized into infinitesimally small segments, and the aforementioned process can be described by the following equations:

$$(v_i(t+1), h_i(t+1)) = f(v_i(t), h_i(t), v_{i-1}(t)) \quad (1)$$

where  $v_i(t)$ ,  $h_i(t)$ ,  $v_{i-1}(t)$  respectively represent the velocity, headway of vehicle  $i$ , and the velocity of the preceding vehicle  $i-1$  at time  $t$ ;  $f(\cdot)$  denotes the state transition function.

In real-world scenarios, different drivers commonly exhibit markedly diverse behaviors when faced with identical situations. This variability is intricately associated with individual driving habits, short-term fluctuations in the surrounding environment, and specific driving intentions.

These short-term trajectories serve as external manifestations of driver characteristics, encapsulating abundant driving semantic information. Consequently, they are employed for the identification and differentiation of heterogeneity among drivers. Therefore, the problem is defined as follows:

$$\begin{aligned} dc_i(t) &= f_{dc}(x_i(t-P), x_i(t-P+1), x_i(t)) \\ v_i(t+1), h_i(t+1) &= f_{sp}(v_i(t), h_i(t), dc_i(t), v_{i-1}(t)) \end{aligned} \quad (2)$$

where  $x_i(\cdot) = [v_i(\cdot), h_i(\cdot), \Delta v_i(\cdot), a_i(\cdot), l_i]$ ,  $\Delta v_i(\cdot)$ ,  $a_i(\cdot)$ ,  $l_i$  respectively represent the velocity difference, acceleration, and vehicle length of vehicle  $i$ ;  $P$ ,  $f_{dc}(\cdot)$ ,  $dc_i(\cdot)$  respectively represent the length of historical trajectories, the mapping relationship between trajectories and driving characteristics, and the driving characteristics extracted from information containing  $P$  trajectory samples.

As illustrated in Eq. (2), the objective in this section revolves finding a mapping. The inputs contain the historical trajectory context, the current explicit state of the vehicle  $i$ , the velocity of the preceding vehicle  $i-1$ , and the outputs contain the prediction velocity and headway of the vehicle  $i$  in next time step. However, the mapping is typically nonlinear, leading to significant computational delays in online optimization for mixed traffic flow. The Koopman operator theory provides an promising approach to tackle this challenge.

### C. Koopman operator theory for state prediction of HDVs

1) *Koopman operator theory*: The Koopman operator theory initially provides an alternative linear dynamic description for the evolution of uncontrollable systems [39]. With slight modifications, the Koopman operator can be applied to controlled systems [45]. Therefore, the evolution of system modeled by Eq. (2) can be expressed by a linear Koopman operator in an infinite-dimensional space. Let  $z_i(\cdot) = [v_i(\cdot), h_i(\cdot), dc_i(\cdot)]^T \in \mathbb{Z}$  represents the state of vehicle  $i$ ,  $\mathbf{v}_{i-1}(t) = v_{i-1}^\infty$  denotes all the velocities in the velocity space  $V$ , the Koopman operator on System corresponding to Eq.(2) with the extended state  $[z_i(t), \mathbf{v}_{i-1}(t)]$  is defined as follows:

$$\begin{aligned} \mathcal{K}\phi(z_i(t), \mathbf{v}_{i-1}(t)) &= \phi(z_i(t+1), \mathbf{v}_{i-1}(t+1)) \\ &= \phi(f_{sp}(z_i(t), \mathbf{v}_{i-1}(t)) + \vartheta \mathbf{v}_{i-1}(t)) \end{aligned} \quad (3)$$

where  $\mathcal{K}$  is the Koopman operator in the infinite-dimensional space;  $\vartheta \mathbf{v}_{i-1}(t) = \mathbf{v}_{i-1}(t+1)$  with  $\vartheta$  being a left shift

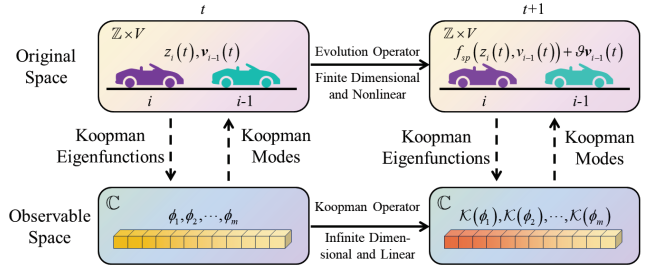


Fig. 1. The relationship between the original space and the observable space

operator. It is noteworthy that, unlike  $f_{dc}(\cdot)$  directly acting on the state  $z_i(\cdot)$ , the Koopman operator  $\mathcal{K}$  operates on the state space functions  $\phi(\cdot) \in \mathbb{Z} \times V$  with  $\phi : \mathbb{Z} \times V \rightarrow \mathbb{C}$ . Exploiting the linearity of  $\mathcal{K}$ , it can be subjected to eigenvalue decomposition, expressed as follows:

$$\mathcal{K}\phi_m(z_i(t), v_{i-1}(t)) = \lambda_m \phi_m(z_i(t), v_{i-1}(t)) \quad (4)$$

where  $\lambda_m$ ,  $\phi_m(\cdot)$  represent the eigenvalues of  $\mathcal{K}$  and their corresponding eigenfunctions, respectively. The future states of the system can be acquired either by directly evolving  $z_i(\cdot)$  or by evolving the complete observable state through the Koopman operator:

$$f_{sp}(z_i(t), \mathbf{v}_{i-1}(t)) = \sum_{m=1}^{\infty} \lambda_m \nu_m \phi_m(z_i(t), \mathbf{v}_{i-1}(t)) \quad (5)$$

where  $\nu_m$  is the Koopman mode corresponding to the eigenvalue  $\lambda_m$ . The relationship between the original space and the observable infinite-dimensional space is depicted in Fig. 1.

Based on Eqs. (3)-(5), the endeavor to derive a global linearized dynamic description equivalent to system modeled by Eq.(2) involves the search for Koopman eigenvalues along with their corresponding eigenfunctions and Koopman modes. Nevertheless, the Koopman operator typically encompasses an infinite number of eigenvalues. Consequently, in most instances, a global linear approximation of the system can only be achieved by identifying essential eigenvalues and their associated eigenfunctions and Koopman modes.

2) *Extended dynamic mode decomposition*: The extended dynamic mode decomposition (EDMD) is a data-driven approach of finding the finite-dimensional approximation  $K$  of the Koopman operator [46]. EDMD employs various basis functions, such as Radial Basis Functions (RBF) with different kernel centers and widths, to represent observable functions. It utilizes least squares regression to calculate  $K$ . For forced dynamics model in Eq. (2), a special way for selecting basis functions is defined in Eq. (5) to obtain :

$$\phi(z_i(t), \mathbf{v}_{i-1}(t)) = [\varphi(z_i(t))^T, \mathbf{v}_{i-1}(t)^T]^T \quad (6)$$

where  $\varphi(\cdot) = [\varphi_1(\cdot)^T, \varphi_2(\cdot)^T, \dots, \varphi_L(\cdot)^T]^T$  represents a set of observable lift functions is general nonlinear. Let  $s_i(k) = \varphi(z_i(k))$ , combining Eqs. (3)-(6), Eq. (7) is obtained:

$$\begin{aligned} \phi(z_i(k+1)) &= \mathcal{K}\phi(z_i(k), \mathbf{v}_{i-1}(k)) \\ &= K [s_n(k)^T \mathbf{v}_{i-1}(k)^T]^T + r \end{aligned} \quad (7)$$

where  $r$  is residual term that describes the gap between the  $L$ -dimensional approximation of the observable space and the

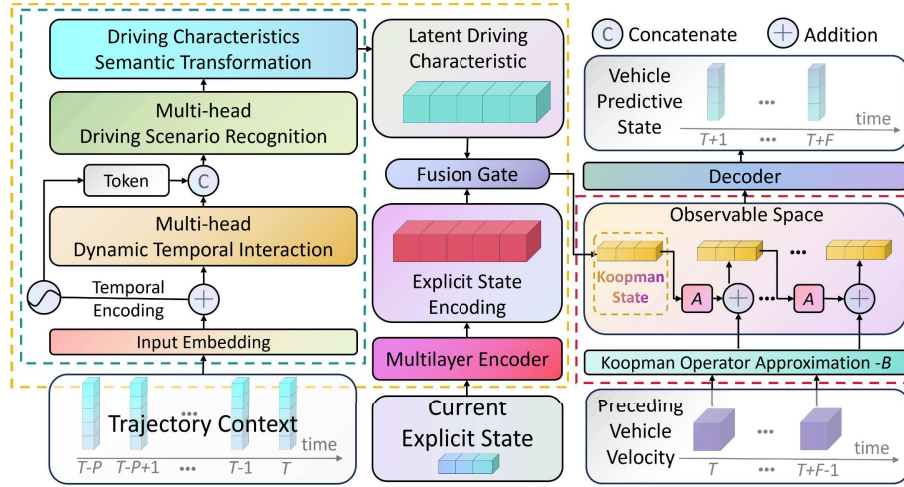


Fig. 2. The model architecture of AdapKoopnet

actual lifted space of the Koopman operator, used to determine the optimal  $K$ . However, selecting the lifting functions for the complex dynamics of System (2) poses a challenge, and advanced deep learning techniques are employed to learn  $K$ .

#### D. Model architecture

A deep learning model, based on attention mechanisms and feedforward networks, is constructed to accomplish the following tasks: 1) Extracting latent driving characteristics from historical trajectory context, which are utilized to aid in understanding and predicting the behavior of HDVs; 2) Learning Koopman lifting functions, Koopman operator approximation, and Koopman modes, the latter two of which are linear, for online optimization in CAVs.

The model architecture is depicted in Fig.2. For trajectory context inputs, the model incorporates a driving characteristic semantic extraction block (highlighted by the deep green dashed box in Fig.2). To handle the current vehicle state input, a multi-layer perceptron-based encoder-lifting function approximation is employed. The fusion gate mechanism integrates the encoding of driving characteristics with the explicit state encoding of the lifting space, yielding the state of the observable high-dimensional Koopman space approximation. By incorporating the future velocity of the preceding vehicle into the network, the model adaptively learns the Koopman operator approximation and achieves multi-step state predictions in the high-dimensional space. This module is denoted as the Koopman evolution block, highlighted by the pink dashed box in Fig.2. Additionally, a linear decoder, serving as an approximation for Koopman modes, is utilized to transform observations from the high-dimensional space to obtain predicted states in the original space.

1) *Driving characteristic semantic extraction block*: As shown in Fig. 2, this block takes trajectory context as input, containing details as specified in the Eq. (2), and outputs a vector representing the current latent driving characteristics of the driver. The block comprises an input embedding and temporal encoding (ITE) module, a multi-head dynamic temporal interaction (DTI) module, a multi-head driving scenario recognition (DSR) module, and a driving characteristics

semantic transformation (DCSE) module, each of which is detailed below.

**Input Embedding and Temporal Encoding (ITE) Module** The input embedding layer serves to convert the trajectory context into a high-dimensional dense representation, allowing the model to comprehensively learn the trajectory features and analyze correlation between trajectory samples. The embedding is achieved through a fully connected layer with a ReLU activation function. Given that the embedding operation is conducted for each trajectory sample, a relative time encoding method is introduced to enable subsequent modules to recognize the temporal information of trajectory context [47]. The expression is as follows:

$$\begin{aligned} TE_{(t,2i)} &= \sin\left(\frac{t}{10000^{(2i/d_{\text{model}})}}\right) \\ TE_{(t,2i+1)} &= \cos\left(\frac{t}{10000^{(2i/d_{\text{model}})}}\right) \end{aligned} \quad (8)$$

where  $i, t$  represent the encoding feature dimension index and time step, respectively;  $d_{\text{model}}$  represents the dimensionality of the encoding of each module in the AdapKoopnet, without special declaration. Subsequently, the trajectory context input embedding and temporal encoding are added together to form the output of this module. The expression is as follows:

$$H_{ITE} = \text{ReLU}(W_{IE} \cdot (x(T-P), \dots, x(T)) + b_{IE}) + TE \quad (9)$$

where  $W_{IE}, b_{IE}$ , represent the weights and biases of the input embedding layer.

**Multi-Head Dynamic Temporal Interaction (DTI) Module** The vehicle state undergoes continuous changes, and there exists a strong interaction and correlation between trajectory samples. This module leverages multi-head attention and feedforward layers to capture and understand the temporal interactions and dependencies within the vehicle trajectory context. Firstly, the multi-head attention mechanism projects the output of ITE into multiple subspaces. In each subspace, it independently learns interaction features within the trajectory context and facilitates feature exchange. By focusing on different subspaces, the model can better capture information from different dimensions within the trajectory context, enhancing its ability to model complex relationships between trajectory sequences. This approach not only accelerates the

speed of training and inference but also contributes to a more comprehensive understanding of the intricate dynamics among trajectory samples.

The dimension of each subspace is also a hyperparameter. In AdapKoopnet, a uniform subspace dimension is adopted and denoted as  $d_{att}$ . The calculation formula for  $\bar{H}_{DTI}$  in the figure is as follows:

$$\begin{aligned} Q_{DTI}^h &= W_{DTI-q}^h H_{ITE} & K_{DTI}^h &= W_{DTI-k}^h H_{ITE} \\ V_{DTI}^h &= W_{DTI-v}^h H_{ITE} \\ \bar{H}_{DTI}^h &= \text{softmax} \left( \frac{Q_{DTI}^h K_{DTI}^h}{\sqrt{d_{att}}} \right) V_{DTI}^h \\ \bar{H}_{DTI} &= LN (W_{DTI-att} (\|_{g=1}^H \bar{H}_{DTI}^h) + H_{ITE}) \end{aligned} \quad (10)$$

where  $W_{DTI-q}^h$ ,  $W_{DTI-k}^h$ ,  $W_{DTI-v}^h$ ,  $W_{DTI-att}$  represents learnable weights;  $\| \cdot$  denotes the concatenate operation.  $LN(\cdot)$  stands for Layer Normalization, a technique that normalizes the trajectory encoding along the feature dimension to mitigate the impact of internal covariate shift [48]. Unlike Batch Normalization (BN), Layer Normalization is more flexible as it is not influenced by the size of the data batch.

After achieving feature exchange within the trajectory context through the attention layer, the feedforward layer is employed for the nonlinear transformation of trajectory encoding. This aims to capture the nonlinear relationships within the trajectory context, facilitating the model in learning higher-level abstract representations. The feedforward layer consists of two linear transformations and an activation function. Initially,  $\bar{H}_{DTI}$  undergoes a fully connected layer, followed by the application of the ReLU activation function, and finally passes through another fully connected layer. After  $\bar{H}_{DTI}$  goes through the feedforward layer, the output of the DTI module is obtained, calculated using the following formula:

$$\begin{aligned} H_{DTI} & \\ &= LN (W_{DTI}^{FN-2} \cdot \text{ReLU} (W_{DTI}^{FN-1} \cdot \bar{H}_{DTI}) + \bar{H}_{DTI}) \end{aligned} \quad (11)$$

where  $W_{DTI}^{FN-1}$  and  $W_{DTI}^{FN-2}$  represent the weights of the feedforward layer in the DTI module.

### Multi-Head Driving Scenario Recognition (DSR) Module

Following the extracting and initial abstracting of temporal interaction characteristics within the trajectory context through the DTI module, the cognitive understanding of driving scenario and the extraction of driving characteristic semantics become crucial steps. This is because, in different driving scenarios, even for the same driver, driving characteristics may vary. For example, in scenarios with large headway, drivers may not require to remain highly vigilant about their preceding vehicles, and their driving behavior tends to be smoother. Conversely, in high-density and high-velocity scenarios, drivers may concentrate more on monitoring changes in the state of preceding vehicle and respond more actively. The DSR module learns scenario information hidden within the trajectory context by adapting to relevant feature variations from a vast set of driving trajectory contexts. It dynamically recognizes and classifies the driving scenario in which the vehicle is situated.

Fig. 3 (a) illustrates the structure of the DSR module. Initially, Eq. (8) is utilized to generate a special encoding

token. Subsequently, this token is concatenated with the output of the DTI module  $H_{DTI}$ , functioning as the original query. The role of this token is to extract features conducive to the cognitive understanding of driving scenarios by attending to the trajectory context encoding. These features undergo further abstraction through the nonlinear transformation of the feedforward layer. The module was associated and matched these abstracted features with the learned scenario information features of the model, achieving cognitive recognition and prediction of implicit driving scenarios within the trajectory context. Similar to the DTI module, this module conduct deep exchange and further abstraction of interaction features within the trajectory context.

The computational process of the DSR module is fundamentally similar to the DTI module. Its output in the feedforward layer is as follows:

$$H_{DSR-DS}, H_{DSR-TC} = \bar{W}_{DSR} (SE, H_{DTI}) \quad (12)$$

where  $SE$ ,  $\bar{W}_{DSR}$ ,  $H_{DSR-TC}$  and  $H_{DSR-DS}$  represent the special encoding token, the weights of DSR module, the trajectory context encoding in Figure 4, and the special encoding token that completes the extraction of driving scenario features, respectively.  $H_{DSR-DS}$  undergoes a linear layer to aggregate driving scenario features, resulting in a vector with the same dimension as the predefined number of scenes. After applying the softmax activation function, the driving scenario prediction vector depicted in Fig. 3 (a) is obtained. Each dimension of this vector represents the predicted probability of the trajectory context belonging to the corresponding scene. The formula is expressed as follows:

$$H_{DS} = \text{softmax} (W_{DSR-DS} \cdot (H_{DSR-DS})) \quad (13)$$

**Remark 1:** In this study, real labels for driving scenario are not available. Therefore, the driving scenario recognition process involves a spontaneous classification process by the neural network based on a large amount of trajectory context. At the inception of the network design, the task of the DSR module is to cluster recurring trajectory patterns and interpret the generated clusters as potential scenarios. From a macro perspective, this lays the foundation for extracting semantic characteristics of driving characteristics. In Section 5, explicit features corresponding to each scenario will be visualized, although this may not necessarily be the sole basis for the classification of network.

**Driving Characteristics Semantic Transformation (DCSE) Module** As mentioned in the DSR module, driving characteristics vary across different driving scenarios. The current module aims to perform driving characteristic semantic extraction guided by the predicted results of driving scenario recognition. The structural diagram of module is presented in Fig. 3 (b) .

The process begins by defining learnable feature weights corresponding to each scenario. These weights dynamically learn the importance of each feature in the trajectory context encoding under predefined scenarios, using an extensive training data. The features are then aggregated based on the learned importance, obtaining the relevance of each trajectory sample to driving characteristic extraction in a specific driving

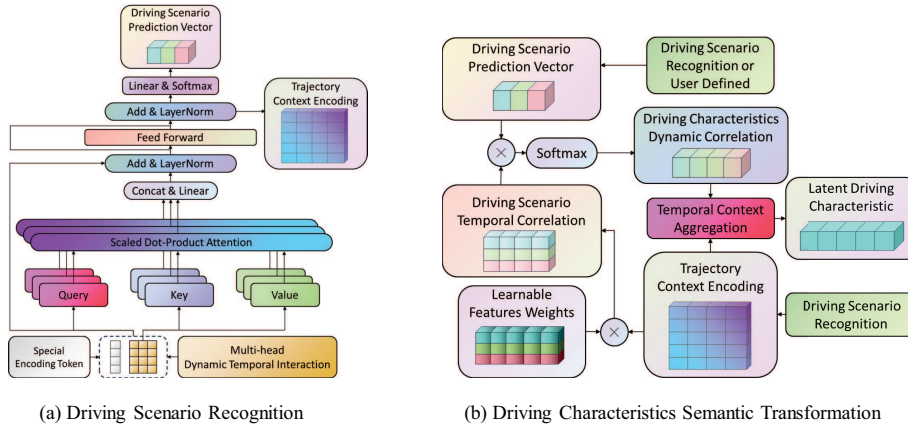


Fig. 3. The architecture of DSR module and DCSE module

scenario. Then, the relevance for each scenario is aggregated based on the probabilities predicted by the DSR module or according to user-defined scenarios. After applying the softmax activation function, the correlation between the trajectory context encoding and driving features is obtained. Based on this correlation, the trajectory context is aggregated, ultimately revealing the driving features hidden within the trajectory context. The computational formula is as follows:

$$dc(T) = \text{softmax}(H_{DSR-TC} ds_{fc} H_{DS})^T H_{DSR-TC} \quad (14)$$

where  $ds_{fc}$ ,  $dc_T$  respectively represent the learnable feature weights corresponding to each scenario, and the latent driving characteristic at time  $T$ .

2) *Explicit state encoder and fusion gate mechanism*: The explicit state encoder is tasked with encoding the explicit state of the vehicle from the original space to an observable high-dimensional space, facilitating the action of the Koopman lifting function on the current vehicle state. This encoder initially embeds the vehicle state into a high-dimensional representation through a linear layer with a ReLU activation function. Subsequently, a Multi-Layer Perceptron (MLP) with tanh activation function is utilized to perform multiple linear transformations on the embedded representation, completing the task of encoding the explicit state of the vehicle. Next, the explicit state encoding and the latent driving characteristics of the vehicle need to be fused to form the Koopman state approximation for the current time step. The Gated Linear Unit (GLU) is introduced to accomplish this fusion task. And the computational formula is as follows:

$$\begin{aligned} es(T) &= W_{ESE} \cdot es(T) \\ s(T) &= W_{FG} \cdot (dc(T), es(T)) \end{aligned} \quad (15)$$

where  $es(T) = (v(T), h(T))^T$ ;  $W_{ESE}$ ,  $W_{FG}$  represents the weights of explicit state encoder and fusion gate mechanism.  $es(T)$ ,  $s(T)$  are the explicit state encoding and Koopman state approximation of the vehicle at time step  $T$ .

3) *Koopman evolution block and decoder*: In the Koopman evolution block, the multi-step evolution in the observable high-dimensional linear system is achieved based on the Koopman operator approximation  $K$  learned through two linear layers without bias. Specifically,  $K$  comprises the system matrix  $A$  and the control matrix  $B$ .  $A$  describes the process of system state transition without control inputs, while the

velocity of preceding vehicle in the prediction horizon is treated as the system control input. This input is applied to the system through the control matrix  $B$  to complete the system evolution. The formal expression of this process is as follows:

$$\begin{aligned} s^P(T+F) &= As^P(T+F-1) + Bv_{-1}(T+F-1) \\ &= A^F s(T) + \sum_{f=1}^F A^{f-1} B v_{-1}(T+F-f) \quad (16) \\ &\triangleq \tilde{A}^F(s(T), v_{-1}(T:T+F-1)) \end{aligned}$$

where  $s^P(\cdot)$ ,  $v_{-1}(\cdot)$  represent the predicted state in high-dimensional space and the velocity of the preceding vehicle, respectively.

Subsequently, the decoder, characterized as a bias-free linear layer, serves to approximate the Koopman modes and reconstruct the predicted state from the observable high-dimensional space to the original space. To minimize online computation delay for CAVs, the decoder is specifically designed as a linear layer without bias (In Section 5, the predictive performance difference between the current decoder and using an MLP as the decoder will be demonstrated). The reconstructed state variables in the original space align with the state variables input to the explicit state encoder in AdapKoopnet. The reconstruction process is expressed as follows:

$$es^P(T+f) = W_{DEC} \cdot s^P(T+f) \quad (17)$$

where  $es^P(T+f) = (v^P(T), h^P(T))^T$  represents the predicted state of the original space;  $W_{DEC}$  represents the learnable weights in the decoder.

**Remark 2:** In a typical trajectory prediction task, incorporating future velocities of the preceding vehicle as inputs may be impractical. However, the primary objective of AdapKoopnet is to predict the response driving behavior of HDVs to the preceding vehicle. This facilitates subsequent inferences about the required velocity of the CAVs. This makes this setup appear much more reasonable.

### E. Loss function

Loss of AdapKoopnet is composed of reconstruction error, prediction error, and linear evolution error [49]. Specifically, the reconstruction error represents the difference between the reconstructed state obtained by embedding the current

explicit state of the vehicle into a high-dimensional space and reconstructing it through the decoder, and the original state. To achieve accurate reconstruction of the original state, the reconstruction error for the entire prediction horizon is included as part of the loss function, expressed as follows:

$$L_C = \frac{1}{F+1} \sum_{f=0}^F \|\varphi^d(\varphi^e(es(T+f))) - es(T+f)\| \quad (18)$$

where  $\varphi^d(\cdot)$ ,  $\varphi^e(\cdot)$  represent the transformations performed by the encoding block (highlighted by the yellow dashed box in Figure 2) and the decoder in AdapKoopnet;  $\|\cdot\|$  represents mean squared error. The prediction error represents the difference between the predicted state and the ground truth, and it is defined as:

$$L_P = \frac{1}{F} \sum_{f=1}^F \|es^P(T+f) - es(T+f)\| \quad (19)$$

The linear evolution error represents the difference between the Koopman state approximation at time  $T$  after  $F$  steps of linear evolution and the Koopman state approximation at time  $T+F$ . It is defined as:

$$L_E = \|s^P(T+F) - s(T+F)\| \quad (20)$$

The loss function of AdapKoopnet is expressed as:

$$L = \alpha_C L_C + \alpha_P L_P + \alpha_E L_E \quad (21)$$

where  $\alpha_C$ ,  $\alpha_P$ ,  $\alpha_E$  are the weights corresponding to the three parts of the loss, and they are hyperparameters. To avoid manually selecting hyperparameters, Dynamic Weight Average (DWA) are introduced [50]. These weights are adjusted based on the losses from the previous epoch in the dynamic loss function.

#### IV. ADAPKOOPPC: PREDICTIVE CONTROL FRAMEWORK OF CAVS FOR REAL-TIME OPTIMIZING MIXED TRAFFIC FLOW BASED ON ADAKOOPNET

##### A. Problem description and system state representation

Consider a local traffic flow within a high-density mixed traffic flow, as illustrated in Fig. 4 consisting of  $N$  HDVs and  $G$  CAVs driving in the same lane. The leading vehicle is a HDV numbered as 0. For convenience, CAVs are sequentially numbered as  $1, 2, \dots, G$ . The HDVs located between CAV  $g$  and  $g+1$  are sequentially numbered as  $g_1, g_2, \dots, g_{n_g}$ . The equivalence relationships exist:  $\sum_{g=1}^G g_{n_g} = N$ . Assuming that all HDV states in this local traffic flow can be collected through the onboard sensors of CAVs or a V2X (Vehicle-to-Everything) system. The control problem of the local traffic flow is defined as achieving the following objectives through the rolling optimization of control inputs for CAVs: (1) Minimizing the velocity difference between any two adjacent vehicles in the local traffic flow, while maintaining reasonable headway to alleviate traffic oscillations transmitted by the leading vehicle. (2) Ensuring that the velocities of vehicles in the local traffic flow are close to that of the leading vehicle, aiming to mitigate oscillations while maintaining traffic efficiency.

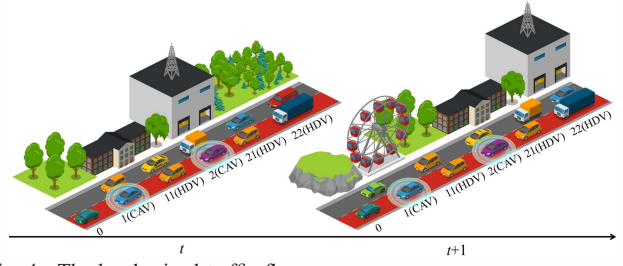


Fig. 4. The local mixed traffic flow

For the convenience of constraint formulation, the local traffic flow state is defined as follows:

$$ES(t) = (p_1(t), v_1(t), a_1(t), es_{11}^T(t), \dots, es_{Gn_G}^T(t)) \quad (22)$$

where  $ES(t)$  encompasses the headways, velocities of all vehicles in the local traffic flow, as well as the velocity differences of HDVs and accelerations of CAVs;  $p_1(t)$  is the position of the first CAV in the local traffic flow. The control input of the local traffic flow is defined as the jerk of CAVs, i.e., the rate of change of acceleration, denoted as:

$$U(t) = (u_1(t), u_2(t), \dots, u_G(t)) \quad (23)$$

**Remark 3:** In large-scale high-density mixed traffic flow scenarios, the lane-changing frequency is low, areas without lane changes occur can be divided into multiple local traffic flow as described above. The local traffic flow lacks a strict organizational structure, requiring cooperation among a few neighboring CAVs to establish. Unlike most existing research, the achievement of control objectives of the local traffic flow does not depend on the so-called equilibrium velocity and equilibrium headway. Minimizing the velocity difference between adjacent vehicles is more readily accepted by HDV drivers, aligns with their own driving objectives in most cases. For scenarios with low penetration rates of V2X systems, simulation experiments relying solely on the onboard sensors of CAVs are conducted and tested in Section 6.

##### B. State predictive model of mixed traffic flow

To enable the rapid convergence of the local traffic flow to the desired state while satisfying the constraints on local traffic flow states and control inputs, a predictive control framework is adopted. The framework assumes a set of feasible control input sequences within a specified region known as the control horizon  $N_C$ . Based on the predictive model, a series of predictive states within the predictive horizon  $N_P$  is obtained. By minimizing the error between the reference state and the predictive state, the optimal control input that satisfies constraints is determined. The current step control input is then applied to the CAVs, and this iterative process ensures that the control input at each step for the CAVs is at least a suboptimal solution. It is evident that in this framework, the accuracy of the local traffic flow state predictive model is crucial. Firstly, the CAVs in the local traffic flow are controllable, and



their predictive state is obtained through the following vehicle kinematics equations:

$$\begin{aligned} p_q(t+1) &= p_q(t) + v_q(t) \cdot \Delta t \\ v_q(t+1) &= v_q(t) + a_q(t) \cdot \Delta t \\ a_q(t+1) &= a_q(t) + u_q(t) \cdot \Delta t \end{aligned} \quad (24)$$

$$= A_{CAV} \cdot \begin{bmatrix} p_q(t) \\ v_q(t) \\ a_q(t) \end{bmatrix} + B_{CAV} \cdot u_q(t)$$

where  $A_{CAV} = \begin{bmatrix} 1 & \Delta t & 0 \\ 0 & 1 & \Delta t \\ 0 & 0 & 1 \end{bmatrix}$ ,  $B_{CAV} = \begin{bmatrix} 0 \\ 0 \\ \Delta t \end{bmatrix}$  represent the local traffic flow matrix and state matrix of CAVs, respectively. In this local traffic flow, there is always at least one CAV in front of any HDV. Therefore, AdapKoopnet can be cascaded to predict the states of all vehicles under specific control inputs of CAVs. This forms the basis for resolving traffic flow stop-and-go waves. The predictive process for all HDVs is illustrated in Fig. 5. Prior to the predictive process, it is necessary to obtain the high-dimensional representation of the current state of the vehicles using the encoding block of AdapKoopnet.

However, the predictive process seems to be cumbersome, particularly when local traffic flow involves numerous vehicles. Therefore, the state predictive model needs to be integrated before initiating prediction to perform parallel prediction of all vehicle states within the local traffic flow. For any HDV in local traffic flow, the following relationship exists:

$$\begin{cases} s_{gn_g}(t+1) = A \cdot s_{gn_g}(t) + B \cdot v_{gn_g-1}(t) \\ es_{gn_g}(t) = C \cdot s_{gn_g}(t) \end{cases} \quad (25)$$

where  $C$  is the observation matrix, which is the linear decoder in AdapKoopnet. For the HDVs, when the preceding vehicle is also an HDV, the following equations are further obtained:

$$s_{gn_g}(t+1) = A \cdot s_{gn_g}(t) + B \cdot C_v \cdot s_{gn_g}(t) \quad (26)$$

where  $C_v$  represents the row in the observation matrix used for observing velocity. Combining Eqs. (22)-(26), the predictive model for the local traffic flow is obtained:

$$\begin{cases} S(t+1) = A_S \cdot S(t) + B_S \cdot U(t) \\ ES(t) = C_S \cdot S(t) \end{cases} \quad (27)$$

where

$$S(t) = [p_1(t), v_1(t), a_1(t), s_{11}(t), \dots, s_{GN_G}(t)]^T$$

$$A_S = \begin{bmatrix} A_{CAV} & & & & & \\ B & A & & & & \\ & BC_v & A & & & \\ & & \ddots & \ddots & & \\ & & & & A_{CAV} & \\ & & & & \ddots & \ddots \end{bmatrix} \quad (28)$$

$$B_S = \begin{bmatrix} B_{CAV} & & & & & \\ & \ddots & & & & \\ & & & & & \\ & & & & & \\ & & & & & B_{CAV} \end{bmatrix}, C_S = \begin{bmatrix} I_3 & & & & & \\ & C & & & & \\ & & \ddots & & & \\ & & & & & \end{bmatrix}$$

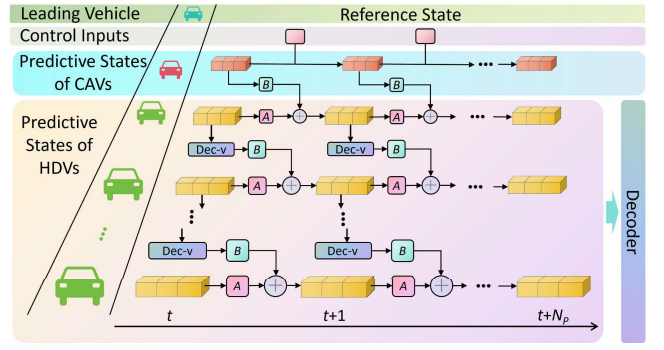


Fig. 5. State Predictive Process of Mixed Traffic Flow

### C. AdapKoopPC for mixed traffic flow

1) *Constrained optimization problem of mixed traffic flow:* Assuming the predictive horizon is the same as the control horizon and denoting it as  $N_P$ , at time  $t$ , the optimization objective for the mixed traffic flow defined in Section 4.1 can be formulated as minimizing the following cost function over the horizon to find an optimal set of control inputs  $U^*(t) = [U^*(0|t), U^*(1|t), \dots, U^*(N_P-1|t)]^T$ :

$$J = \sum_{i=1}^{N_P} \|ES(i|t) - ES_{ref}(t+i)\|_Q^2 + \|U(i-1|t)\|_R^2 \quad (29)$$

where  $ES(i|t)$  is the predictive state of the local traffic flow after time steps  $i$  at time  $t$ ;  $ES_{ref}(t)$  represents the reference state, it provides the reference values for the velocity of CAVs in the local traffic flow, namely the average velocities of their respective preceding vehicles over the time interval  $t - N_P$  to  $t$ ;  $Q$  and  $R = r_u \cdot I_G$  are diagonal matrices, representing the penalty weights for state and control input, respectively, where  $Q$  contains penalties for velocities of CAVs and velocity differences of HDVs, defined as follows:

$$Q = \begin{bmatrix} q_{CAV} & & & & & \\ & q_{HDV} & & & & \\ & & \ddots & & & \\ & & & & q_{HDV} & \\ & & & & & \end{bmatrix} \quad (30)$$

$$q_{CAV} = \begin{bmatrix} 0 & & & \\ & q_{CAV}^2 & & \\ & & 0 & \\ & & & \end{bmatrix}, q_{HDV} = \begin{bmatrix} 0 & & & \\ & 0 & & \\ & & & q_{HDV}^{\Delta v} \end{bmatrix}$$

Additionally, the local traffic flow states and control inputs must satisfy the following constraints:

$$\begin{aligned} h_{\min} &< h(t) < h_{\max} \\ v_{\min} &< v(t) < v_{\max} \\ a_{\min} &< a_{CAV}(t) < a_{\max} \\ u_{\min} &< u(t) < u_{\max} \end{aligned} \quad (31)$$

These constraints respectively imply that the headways of all vehicles in the local traffic flow should remain within a reasonable range, velocities should stay within velocity limits, and the acceleration and control inputs of CAVs should adhere to vehicle dynamics constraints.

2) *Standard quadratic programming of AdapKoopPC:* To facilitate solving, the constrained optimization problem of mixed traffic flow can be reformulated as a standard quadratic programming problem. Building on the linear model described

in Eq. (25), the predictive states among the future  $N_P$  steps can be expressed as:

$$\mathbf{ES}(t) = \mathbf{AS}(t) + \mathbf{BU}(t) \quad (32)$$

where  $\mathbf{ES}(t) = [ES(1|t)^T, \dots, ES(N_P|t)^T]^T$ ;  $\mathbf{BU}(t) =$

$$[U(0|t)^T, \dots, U(N_P - 1|t)^T]^T; \mathbf{A} = \begin{bmatrix} C A_S \\ \vdots \\ C A_S^{N_P} \end{bmatrix}^T; \mathbf{B} =$$

$$\begin{bmatrix} C_S B_S & & & & & \\ C_S A_S B_S & C_S B_S & & & & \\ \vdots & \vdots & \ddots & & & \\ C_S A_S^{N_P-1} B & C_S A_S^{N_P-2} B & \dots & C_S B_S & & \end{bmatrix}.$$

Let  $\mathbf{ES}_{\text{ref}}(t) = [ES_{\text{ref}}(1|t)^T, \dots, ES_{\text{ref}}(N_P|t)^T]^T$ ,  $\mathbf{Q} = I_{N_P} \otimes \mathbf{Q}$ ,  $\mathbf{R} = I_{N_P} \otimes \mathbf{R}$ , where  $\otimes$  is Kronecker product. And by discarding the terms without  $\mathbf{U}(t)$ , the cost function Eq. (29) has been rewritten as follows:

$$J = \frac{1}{2} \mathbf{U}(t)^T \mathbf{H} \mathbf{U}(t) + \mathbf{F}^T \mathbf{U}(t) \quad (33)$$

where  $\mathbf{H} = 2(\mathbf{B}^T \mathbf{Q} \mathbf{B} + \mathbf{R})$ ;  $\mathbf{F}^T = 2(\mathbf{A} \mathbf{S}(t) - \mathbf{ES}_{\text{ref}}(t))^T \mathbf{Q} \mathbf{B}$ . Optimal control input can be got by solving the constrained optimization problem (33) subject to Eqs. (31) and (32).

## V. EXPERIMENT PART I: ADAPKOOPNET FOR CAR FOLLOWING TRAJECTORY PREDICTION OF HDVs

### A. Dataset description and evaluation metrics

The performance of AdapKoopnet model is evaluated on the HighD dataset, which is a large-scale naturalistic vehicle trajectory dataset collected from German highways. The car-following trajectory dataset is extracted in accordance with the criteria presented in [28], includes 18396432 records. And the root mean square error (RMSE) is selected as the evaluation metrics:

$$RMSE = \sqrt{\frac{1}{\Gamma} \sum_{i=1}^{\Gamma} (y_i - \bar{y}_i)^2} \quad (34)$$

### B. Baseline models and experiment settings

The performance of designed AdapKoopnet for HDVs car following trajectory Prediction is compared and evaluated with the following baseline models.

**MLP** utilizes a multi-layered nonlinear fully connected neural network to predict the car-following trajectory of vehicle.

**LSTM** utilizes LSTM-based encoder-decoder architecture to predict vehicle trajectories [51].

**Koopnet** is an ablation version of AdapKoopnet where the extraction of driving characteristics semantic information from the trajectories context of vehicle is eliminated.

**N-AdapKoopnet** is a variant of AdapKoopnet where the decoder is replaced with fully connected layers featuring non-linear activation functions.

**N-Koopnet** features an encoder composed of fully connected layers with non-linear activation functions.

**S-AdapKoopnet** employs a modified architecture in which the width of each layer is halved compared to AdapKoopnet

while retaining the same structure. This modification aims to reduce the computational load, especially when implementing optimization for large-scale mixed traffic flow.

PyTorch 2.1.0 framework is utilized to construct the predictive model, and end-to-end training was performed under a platform with Intel Core i9-13900K processor and NVIDIA RTX 4090 GPU. The processed car-following trajectories were split into training, validation, and test sets in a ratio of 7:1:2. The model relevant hyperparameters are detailed in Table I.

TABLE I  
MODEL HYPERPARAMETER

Hyperparameter Type	Hyperparameter	Values
Explicit State Encoder	Number of Layers	3
	MLP activation function	Tanh
	Dropout	0.2
Semantic Extraction Block	Trajectory Context horizon	31
	Driving Scenario type	3
	Attention head	4
	Attention dimension	64
	Input feature dimensione	5
Other hyperparameters	Model dimension	128
	Prediction horizon	15
	Batch size	256
	Max train epochs	25
	learning rate(LR)	$10^{-5}$
	LR scheduler	Exponent
	LR decay rate	0.6

### C. Trajectory prediction experiment results

#### 1) HDVs trajectory prediction performance comparison:

Table II statistics the performance index results of AdapKoopNet and baseline models for trajectory prediction under different prediction horizons. In terms of velocity, when the prediction step is 5 (0.6 seconds), the RMSE of LSTM is the smallest at 0.084m. The reason may be due to the architectural design of the LSTM encoder-decoder and the excellent gate control unit structure, which has advantages in short time domain prediction. When the prediction step increases to 1.2 seconds, AdapKoopNet has a significant advantage, with an RMSE of 0.145, which means it has better long-term prediction ability. AdapKoopnet considers the multi-step evolution loss of linear space during the training process, giving up some short-term prediction performance in exchange for the average prediction performance in the entire prediction time domain. Although Koopman theory provides a global linear expression of a dynamic system in an infinite-dimensional space, AdapKoopnet ultimately implements predictions in a finite-dimensional (128-dimensional) space, which is bound to be affected by linear systems, resulting in some losses. Simply put, with the help of the powerful feature extraction capability of the attention mechanism and the adaptive driving feature extraction architecture based on driving scenarios, the AdapKoopnet series models have achieved performance comparable to LSTM in terms of short-term prediction performance, and better than it in terms of long-term prediction performance.

As the prediction step further increases, N-AdapKoopNet outperforms AdapKoopNet in performance, reflecting the loss of prediction performance caused by the adoption of linear decoders, the average performance at each prediction step size is still the most outstanding for AdapKoopNet. Subsequently,

comparing the distance between the front of the vehicle, the most effective models are LSTM and N-AdapKoopNet. However, the decoder of this model is non-linear and can indeed achieve good trajectory prediction results. However, it is also not suitable for subsequent CAVs prediction control. Taking into account the accuracy of trajectory prediction and the feasibility of subsequent control for real-time traffic flow optimization, it is evident that AdapKoopNet has significant advantages. In addition, in order to balance prediction performance and inference cost, the large-scale traffic flow simulation experiment in Section 6.3 is based on S-AdapKoopnet.

Fig. 6 (a) shows the indicator line graph of AdapKoopNet and the baseline models under complete 15 prediction steps, where the red line represents AdapKoopNet. The comparison results mainly including the following two aspects. Firstly, regardless of the prediction range, the AdapKoopNet model outperforms KoopNet, indicating that it effectively and accurately captures the underlying data features and achieving personalized driving behavior prediction. Secondly, as the prediction range increases, although the prediction performance of AdapKoopNet has declined, it still maintains accuracy and feasibility. The comparative analysis with the baseline models is similar to Table II and will not be further elaborated.

Fig. 6 (b) focuses specifically on the prediction step scene of 1.8s. 300 batches are randomly selected from the test set, and the predicted and true values of headway and velocity are visualized, with the color axis representing the probability density. It can be observed that the velocity of most trajectory appears between 20 and 30 meters, while the headway remains around 30 to 50 meters. In addition, the vast majority of trajectory samples are attached near the diagonal, which means that the predicted values are very close to the true values, reflecting the strong ability of AdapKoopNet to capture trajectory evolution features and make accurate predictions. Of course, there are some samples with significant deviations, but the density of these samples is extremely low and almost does not affect the overall trajectory prediction performance. Besides, benefiting from the rolling optimization method adopted in the AdapKoopPC, the negative impact of these deviation samples can be ignored.

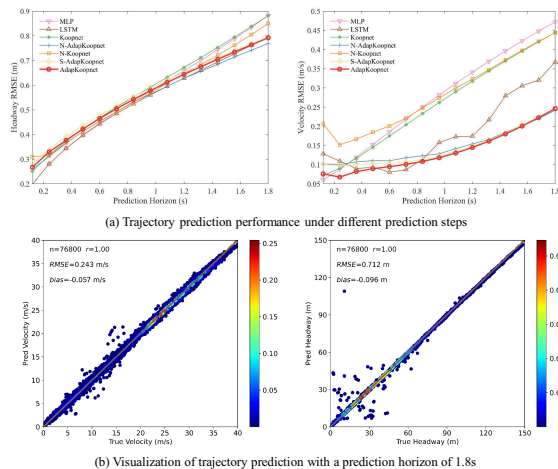


Fig. 6. HDVs driving state prediction performance of the AdapKoopnet

2) *Potential scenarios recognition and clustering results:* Furthermore, in order to verify the effectiveness of AdapKoopnet in directly extracting potential driving scenarios from real trajectory data and adaptively learning driving characteristics without any pre-define or pre-label, a series of visualizations of the model training results are performed.

The first thing to explore is what all trajectory samples output after passing through the multi-head driving scenario recognition module. Fig. 7 shows the distribution of trajectory samples for various driving scenarios learned and clustered. Fig. 7 (a), (b) and (c) show the headway-velocity relationship of trajectory samples under three driving scenarios. The color axis represents the proportion of samples, with the proportion of trajectory samples increasing as the color approaches red. It is obvious that Fig. 7 (a) tends towards medium to high velocity driving scenario, with the highest proportion of sample clusters distributed at velocity of around 25m/s, accompanied by a moderate headway of 30 meters to 60 meters. The distribution of trajectory samples in Fig. 7 (b) is relatively uniform, including scenario with small headway at low velocity and large headway at high velocity. Fig. 7 (c) corresponds to the third driving scenario, where the overall trajectory exhibits low velocity accompanied by small headway. Fig. 7 (d), (e), and (f) depicts the relationship between the average velocity difference, average headway, and average velocity of trajectory samples in three driving scenarios, with the color axis representing velocity. Significantly, all trajectory samples are clearly clustered into three driving scenarios, each with similar repetitive patterns. Of course, the characteristics of all trajectories in each posture scenario are not entirely the same. Overall, AdapKoopNet can adaptively extract features from a large number of trajectory samples and cluster them, ultimately forming these three potential driving scenarios.

3) *Scenario inherent temporal correlation and the driving characteristics dynamic temporal correlation:* Fig. 8 reveals this specific driving scenario inherent temporal correlation and the driving characteristics dynamic temporal correlation. 8 (a) corresponds to the output of the driving characteristics semantic module shown in 3 (b) in AdapKoopNet. It is worth noting that as mentioned earlier, AdapKoopNet adaptively learns the feature weights of each trajectory sample belonging to three different scenarios, and then clusters them into potential scenarios according to their propensity. Therefore, more precisely, what is extracted here is the inherent temporal correlation corresponding to each driving scenario. Specifically, driving scenario 1 and driving scenario 3 are quite similar, both reflecting an overall trend of lower temporal correlation as the historical time step increases. The difference lies in that the former is not as extreme as the latter, and Scenario 3 strongly relies on the nearest time step and has almost no correlation on distant historical trajectories. There is a significant difference between driving scenario 2 and the above two driving scenarios, characterized by a more stable temporal correlation on the historical trajectory of each time step, rather than being more affected as time approaches.

Fig. 8 (b) indicates the dynamic correlation that directly reflects the actual driving characteristics of each vehicle. Here, we visualized six vehicles trajectories in each scenario.

TABLE II  
COMPARISON OF HDVs LONGITUDINAL TRAJECTORY PREDICTION PERFORMANCE INDICATORS

Model	Velocity RMSE(m/s)				Headway RMSE (m)			
	0.6s	1.2s	1.8s	Average	0.6s	1.2s	1.8s	Average
MLP	0.184	0.341	0.472	0.3324	0.447	0.659	0.882	0.663
LSTM	<b>0.084</b>	0.173	0.367	0.208	<b>0.444</b>	<b>0.628</b>	0.797	0.623
Koopnet	0.176	0.318	0.444	0.313	0.468	0.672	0.883	0.674
N-AdapKoopnet	0.110	0.155	<b>0.243</b>	0.169	0.455	<b>0.628</b>	<b>0.769</b>	<b>0.618</b>
N-Koopnet	0.200	0.322	0.444	0.322	0.454	0.647	0.851	0.650
S-AdapKoopnet	0.105	0.148	0.247	0.167	0.477	0.651	0.796	0.641
AdapKoopnet	0.095	<b>0.145</b>	0.2471	<b>0.167</b>	0.466	0.643	0.797	0.634

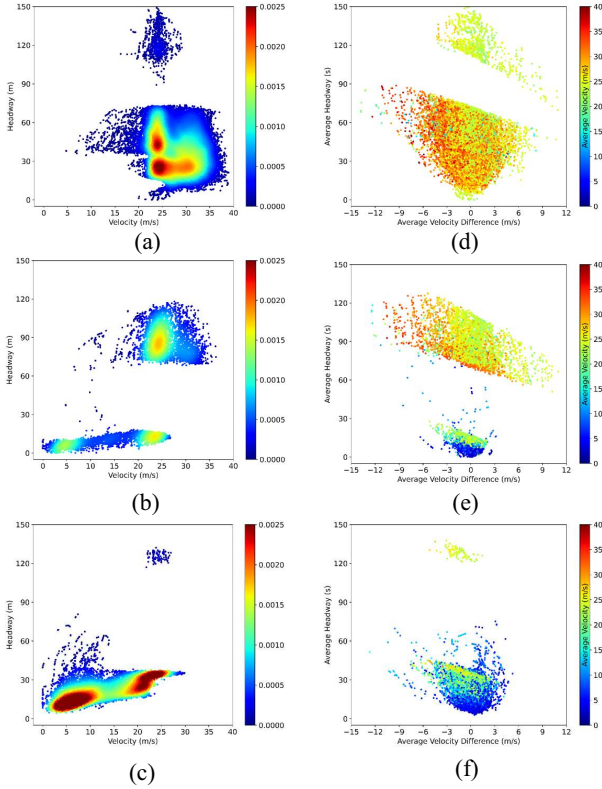


Fig. 7. Adaptive Multi-driving scenario recognition results

Significantly, whether it is driving scenarios 1, 2, or 3, the corresponding six trajectories exhibit dynamic correlations equivalent to the six variants in each driving scenario. They tend towards a scenario and follow the inherent temporal characteristics of the driving scenario, but the driving characteristics of each trajectory are different from each other, corresponding to the driving characteristic dynamic correlation module. These indeed demonstrate that AdapKoopNet has adaptively learned the inherent temporal correlations and driving characteristics dynamic correlations in different driving scenarios. The capture of these correlations contributes to subsequent accurate and personalized trajectory prediction, which is elaborated and proven in the following section.

4) *Validation of scenarios recognition effectiveness*: Fig. 9 is a comparative experiment demonstrating the effectiveness of the multi-head driving scenario recognition module and the driving characteristics semantic transformation module in learning potential driving scenarios and dynamic temporal correlation. Two trajectory test samples were selected, corresponding to adaptive learning of three driving scenario char-

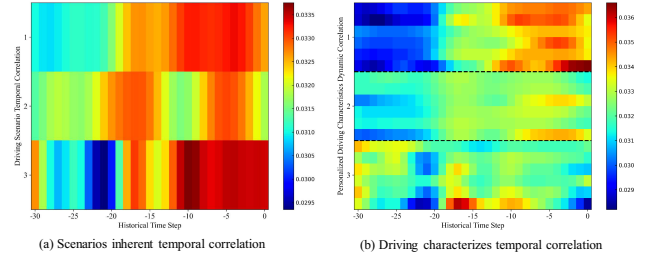


Fig. 8. The inherent temporal correlation of driving scenarios and the temporal correlation of driving characteristics

acteristic weight of 0.012:0.020:0.968 and 0.330:0.151:0.519, corresponding to Fig. 9 (a) and Fig. 9 (b), respectively. A very direct and convincing approach is to manually input different driving scenario labels for the same trajectory, and then compare its trajectory prediction results with those of unlabeled adaptive learning. Firstly, as shown in Fig. 9 (a), the feature weight of driving scenario 3 is 0.968, which is almost close to 1. The predicted trajectory with manually labeled scenario 3 is almost completely consistent with the trajectory prediction results with unlabeled adaptive learning, while the trajectory prediction results in manually labeled driving scenarios 2 and 3 are significantly different. The predicted velocity parameters of the trajectory show the same comparative results. By comparison, Fig. 9 (b) shows that the feature weight of driving scenario 3 learned by AdapKoopNet is 0.519, and the trajectory features are more inclined towards scenario 3. It is obvious that in both headway and velocity aspects, the trajectory prediction results for scenario 3 with manual label driving represented by the yellow line, closely align with the observed values, followed by scenario 1 with manual label, and scenario 2 with manual label has the largest trajectory prediction deviation. The above comparison serves as strong evidence of the effectiveness and superiority of AdapKoopNet. In addition, there is actually another discovery that as the prediction step size increases, the prediction trends under various preset conditions are similar in trajectory prediction. This phenomenon arises from the fact that different prediction conditions correspond to different Koopman operators, with the only variation being the associated feature vectors. This is worth further improvement in future research.

## VI. EXPERIMENT PART II: ADAPKOOOPPC FOR MIXED TRAFFIC FLOW

This section aims to comprehensively evaluate the effectiveness and superiority of the proposed AdapKoopPC in mitigating traffic oscillations in mixed traffic flows. Specifically, it covers small-scale experiments and large-scale experiments.

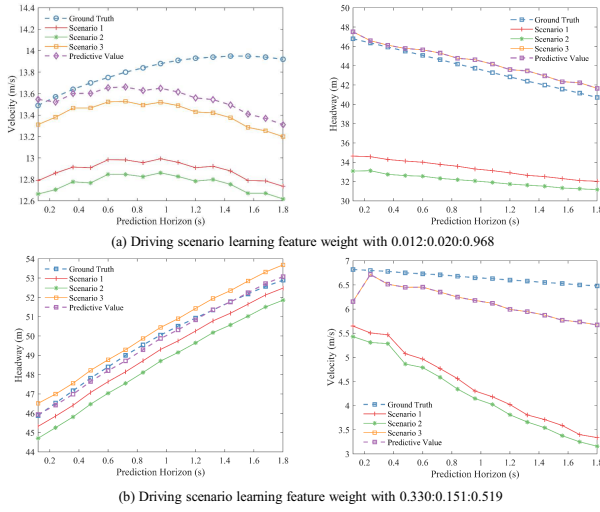


Fig. 9. Trajectory prediction results for the same trajectory under different driving scenario

### A. Simulation settings

The small-scale simulated mixed traffic flow consists of 2 CAVs, 2 HDVs(Truck) and 6 HDVs(Car). The large-scale simulated mixed traffic flow consists of 50 vehicles, of which CAVs and HDVs(Car) account for 80%, and HDVs(Truck) account for 20%. A certain proportion of trucks is set up to build a heterogeneous simulation environment, with the purpose of proving the modeling and prediction capabilities of AdapKoopPC for heterogeneous HDVs. IDM is used as the simulation control model of HDVs, and its parameters are calibrated and obtained from the naturalistic driving dataset using genetic algorithm. The simulation is conducted on an open road, and the head vehicle of the mixed traffic flow evolves according to the following equation to simulate traffic oscillations [52]:

$$v_0(t) = \begin{cases} 25 \text{ m/s} & t \in [0, 4.8] \\ 25 - 5 \sin(0.167(t - 4.8)) \text{ m/s} & t \in [4.8, 180] \end{cases} \quad (35)$$

Except for the first vehicle, which must be a CAV, the arrangement of vehicles in the local traffic flow is randomly generated based on the proportion of vehicle types. The control input for CAVs is solved using the SLSQP optimizer from the Scipy library, and the simulation is conducted on a laptop equipped with the Apple M2 chip. The simulation experiment parameters are shown in Table III.

### B. Real-time control optimization experiment for small-scale mixed traffic flow

The Small-scale experiment aims to validate the effectiveness of AdapKoopnet in balancing traffic flow disturbances and enhancing traffic flow stability, as well as the computational efficiency. The baseline control methods including:

**LTI-MPC:** On the premise that the car-following model adopted by HDVs in the mixed traffic flow is known, linear time-invariant MPC is used to optimize the mixed traffic flow based on the linearized car-following model [18].

**Deep-LCC:** A data-driven non-parametric predictive control framework for mitigating traffic flow velocity oscillations. And the evolution dynamics of mixed traffic flow are learned online using the pre-collected trajectories [18].

TABLE III  
PARAMETER SETTINGS FOR COMPARATIVE EXPERIMENTS WITH DIFFERENT CONTROL METHODS

	Parameter	Value	Parameter	Value	
IDM	$a_{IDM}^{car}$ ( $\text{m/s}^2$ )	1.13	$a_{IDM}^{truck}$ ( $\text{m/s}^2$ )	1.5	
	$b_{IDM}^{car}$ ( $\text{m/s}^2$ )	4	$b_{IDM}^{truck}$ ( $\text{m/s}^2$ )	4	
	$s_0^{car}$ (m)	8.16	$s_{IDM}^{truck}$ (m)	9.66	
	$T_{car}$ (m)	1.13	$T_{IDM}^{truck}$ (m)	1.72	
	$v_{IDM}^{car}$ (m/s)	35.96	$v_{IDM}^{truck}$ (m/s)	54.25	
	$l_{car}$ (m)	4.24	$l_{IDM}^{truck}$ (m)	11.82	
	AdapKoopPC	$h_{min}$ (m)	20	$v_{min}$ (m)	0
		$h_{max}$ (m)	150	$v_{max}$ (m)	150
$u_{min}$ ( $\text{m/s}^3$ )		-6	$u_{max}$ ( $\text{m/s}^3$ )	6	
$q_{HDV}^{\Delta v}$		20	$q_{CAV}^v$	10	
$a_{max}$ ( $\text{m/s}^2$ )		6	$a_{min}$ ( $\text{m/s}^2$ )	-6	
$N_P$		10	$r_u$	2	
Simulation	Duration(s)	180	Interval(s)	0.12	

Additionally, to make a sound comparison of the proposed AdapKoopPC with the baselines, a fixed random seed is setting in the small-scale simulation.

1) *Mixed traffic flow evolution results:* Fig. 10 and Fig. 11 depict and compares the headway and acceleration evolution of small-scale mixed traffic flow under different control methods. The yellow dashed line represents the head vehicle, while the blue and orange thick solid lines represent the two CAVs under various control methods. The remaining 8 vehicles are all HDVs, with HDV8 and HDV10 being trucks and the rest being cars. Fig. 10 (a) and Fig. 11 (a) depict the evolution of the mixed traffic flow corresponding to no control, where the CAV solely considers optimizing its following trajectory with respect to the head vehicle, without taking into account its own guiding influence on the subsequent HDVs. After the head vehicle experiences disturbances starting at 4.8s and begins to oscillate, and the entire traffic flow exhibits substantial acceleration and deceleration. The evolution of the blue line in the middle subgraph indicates that as the CAV decelerates with the leading vehicle, the velocity of the entire mixed traffic flow also begins to oscillate significantly. The following HDVs exhibit significant fluctuations in their headways. Taking the first HDV following behind as an example, the headway drops to 33 meters and then continues to rise to around 72 meters, indicating poor stability due to the promotion of disturbances through the entire traffic flow.

Fig. 10 (b) and Fig. 11 (b) shows the mixed traffic flow evolution after implementing the LTI-MPC. There is a change that needs to be explained in advance, which is that the first CAV did not maintain a constant velocity with the leading vehicle at the beginning. This is because LTI-MPC imposes a penalty on the error between the actual headway and the expected headway. Once there is a small error between the initial headway set in the experiment and the expected headway after traffic flow operates, it will lead to fluctuations in the initial stage of mixed traffic flow evolution, which is difficult to be avoided in the experimental setup. It is obvious that the amplitude of the velocity oscillation of the first CAV also begins to oscillate after receiving the oscillation propagation from the leading vehicle, and the following HDV also oscillates with it. The overall oscillation amplitude decreases relative to Basic-MPC. In terms of headway, taking

the second HDV indicated by the red line as an example, the oscillation amplitude of the headway improved due to the influence of the CAV ahead, reaching a maximum front distance of about 50 meters at 40 seconds. Subsequently, the second CAV also optimized its driving behavior under the action of LTI-MPC, and the trajectories of the following two trucks also fluctuated accordingly, maintaining a distance near the expected headway.

The evolution and improvement of the mixed traffic flow under the Deep-LCC control scenario are shown in Fig. 10 (c) and Fig. 11 (c). Similarly, the initial evolution stage, like the LTI-MPC, requires the first CAV to accelerate in order to achieve equilibrium headway. We can clearly observe that there is little difference between Deep-LCC and LTI-MPC in overall traffic flow evolution improvement, achieving performance comparable to LTI-MPC. The specific details will not be repeated in the description. Of course, Deep-LCC does not require prior knowledge of flow dynamics, and its advantage lies in its data-driven non parametric strategy.

To shift the perspective shifts to Fig. 10 (d) and Fig. 11 (d), the figures show how the mixed vehicleatoon trajectory evolves under AdapKoopPC control. In terms of acceleration, the CAV perceives the oscillation of the leading vehicle and begins to slow down slightly, then maintains a small amplitude of acceleration and deceleration driving behavior, and induces the vehicles behind to maintain a small amplitude of acceleration and deceleration driving behavior. The acceleration evolution is noticeably improved compared to the previous scenario, with the fluctuation range around  $-0.25\text{m/s}$  to  $0.25\text{ m/s}$ . In terms of headway, the headway of CAV is relatively large compared to other previous control methods, but it ensures that the oscillation of the rear HDV headway is significantly reduced, from the previous 30-60 meters to 40-50 meters. This is direct evidence that AdapKoopPC effectively proactively guides and optimizes subsequent HDV driving behavior. It is worth mentioning that the headways of the two trucks after the second CAV fluctuates smoothly and is almost unaffected by the disturbance of the leading vehicle.

Overall, these comparative results further demonstrate that AdapKoopPC can effectively and proactively guide the subsequent HDVs and maintains the smooth driving of the mixed traffic flow. More importantly, whether it is LTI-MPC or Deep-LCC, it is necessary to utilize a given model or simulation to generate some trajectories. However, these trajectories are highly dependent on the expected headway, which has limitations. AdapKoopPC adopts a penalty of velocity difference, which matches the expected goal of most drivers of vehicles in a following state. This will not cause discomfort to the driver and is more conducive to optimize the control of the mixed traffic flow.

2) *Computation time comparison:* Table IV states the real-time computing time for different control methods at each time step, with a time step of 0.12 seconds. The average computation time for LTI-MPC, Deep LCC, and AdapKoopPC is 0.004s, 0.326s, and 0.009s, respectively. To investigate its reasons, LTI-MPC does not require neural network encoding, and the mixed traffic flow state dimension is low, so the solution is the fastest. As for Deep-LCC, it was shown to

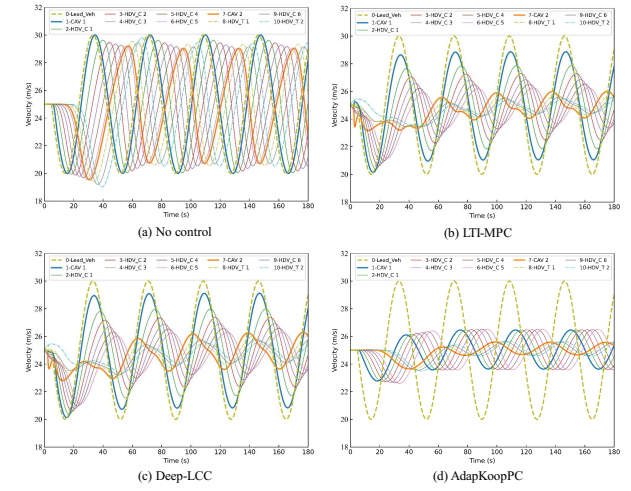


Fig. 10. The mixed traffic flow acceleration evolution comparison under different control methods

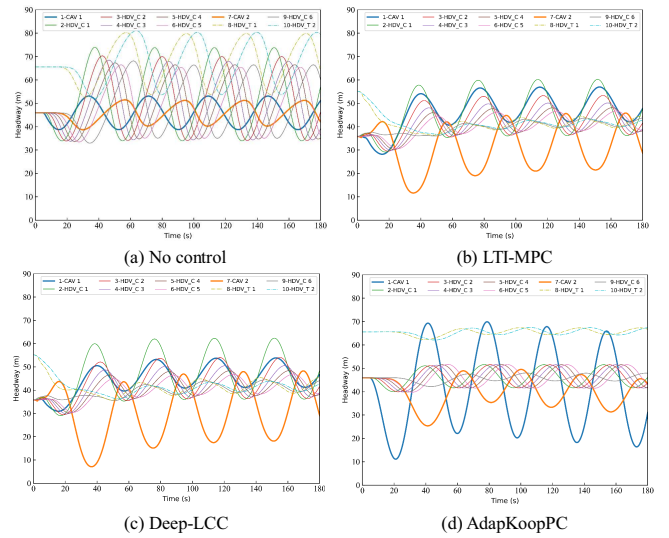


Fig. 11. The mixed traffic flow headway evolution comparison under different control methods

be 0.05s in the previous work. The online computation time of Deep-LCC has shown significant fluctuations in our experiments. When simulating mixed traffic flow scenarios similar to pre-generated trajectory scenarios, the average computation delay is 0.326 seconds. When there is a significant difference between the two scenarios, the model training solution needs to iterate to the maximum number of manually set iterations. Therefore, the delay depends on this value and will not be lower than 0.326 seconds, which may be due to a lack of generalization ability. After the impact of neural network encoding time and significant increase in state dimension, the online computation of AdapKoopPC yields an average time of 0.009 seconds, and the sampling interval is 0.12 seconds, which demonstrates the feasibility of implementing real-time mixed traffic flow control. It is worth mentioning that the simulation experiments of LTI-MPC and Deep-LCC are based on the MATLAB quadprog optimizer, which has better solving performance compared to the SciPy adopted in AdapKoopPC. Therefore, the online computation time of AdapKoopPC can still be further improved.

TABLE IV  
COMPUTATION TIME

Model	LTI-MPC	Deep-LCC	AdaptKoopPC
Computing Time (s)	0.004	0.326	0.009

### C. Real-time control optimization experiment for large-scale mixed traffic flow

This section verifies the ability of AdapKoopPC for large-scale mixed traffic flow control, where the leading vehicle is followed by 50 vehicles. Three types of traffic flow scenarios covering different CAVs penetration rates, communication range degradation, and different CAVs distribution are set up to analyze the effectiveness and performance loss of AdapKoopPC in traffic flow optimization control in a wide range of scenarios.

1) *CAVs penetration rates*: Fig. 12 depicts the overall evolution of the mixed vehicle with AdapKoopPC under different CAV penetration rates, including 0%, 10%, and 20%. Note that there are some white spacing lines, indicating that the trajectory here is a truck trajectory with a greater headway than the headway of the car. The following row shows the corresponding three-dimensional evolution diagram. The experimental comparison results can be mainly summarized into the following two points: a) When there is no CAV in the traffic flow, the disturbance of the leading vehicle propagates directly upstream with the traffic wave, which can be reflected by the increasingly prominent red area in Fig. 12(a). The three-dimensional velocity evolution diagram provides a more intuitive view of the poor driving conditions of the traffic flow. b) As the penetration rate increases to 10%, the traffic wave gradually dissipates and there is no significant fluctuation in the velocity of following vehicles. Until the penetration rate reaches 20%, the velocity oscillation can be almost ignored and maintained around the expected velocity of 25m/s. An experiment with the 30% penetration rate has also been conducted, and its effect is very close to that of 20%, which is not shown here. It can be considered that the effect is approaching saturation at 20% penetration rate. Overall, AdapKoopPC has the ability to significantly alleviate upstream disturbance waves.

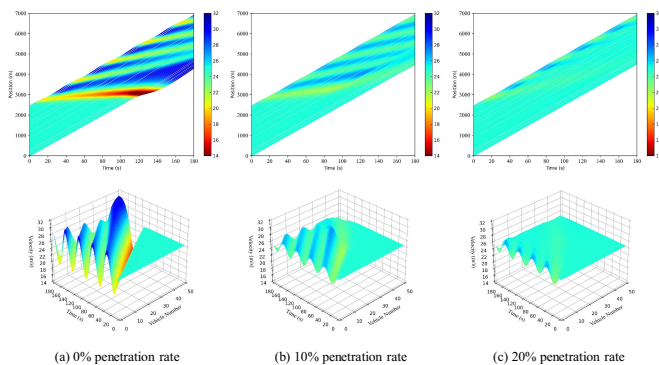


Fig. 12. The mixed traffic flow evolution with AdapKoopPC under different CAVs penetration rates

2) *Communication range degradation*: Another case has also been considered, where CAV deteriorates within communication range due to external factors. The vehicle can only receive information from the following vehicle. And the results

are shown in Fig. 13. Note that more communication restricted scenarios fall between the communication degradation scenario discussed here and the communication lossless scenario, so the control effect of AdapKoopPC in other scenarios will be better than the extreme scenario presented below.

Three penetration rates of 10%, 20%, and 30% are set for experiments under the premise of communication range degradation. Firstly, by comparing Fig. 13 (a) with Fig. 12 (a), AdapKoopPC still plays a significant role, and the traffic oscillation wave generated by the leading vehicle is significantly alleviated. Secondly, the difference between Fig. 13 (a) and Fig. 12 (b) intuitively reflects the impact of communication range degradation on the evolution improvement of the traffic flow. The oscillation slightly increases, indicating that the performance of AdapKoopPC has been slightly degraded. Similarly, in the scenario of a 20% penetration rate, CAV only considers optimizing and inducing the first vehicle behind it, resulting in a decrease in the overall mixed traffic flow evolution effect, which can be observed by comparing Fig. 13 (b) and Fig. 12 (c). Of course, under the above two penetration rates, the traffic flow oscillation propagation is still within an acceptable range, proving that AdapKoopPC can still induce and optimize the performance of the entire traffic flow even under the influence of communication range degradation. Fig. 13 (c) corresponds to a 30% penetration rate. The simulation results confirm that the evolution of the traffic flow is stable and smooth, and the optimization effect is approaching saturation.

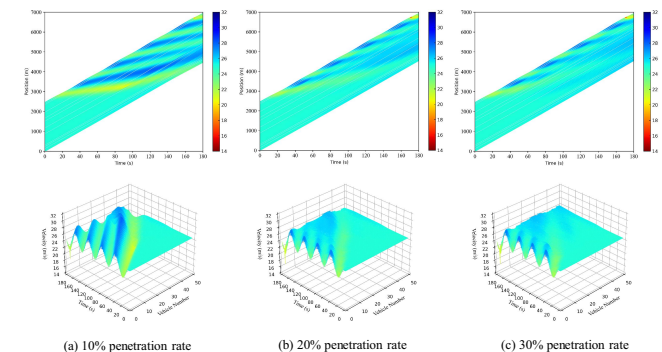


Fig. 13. The mixed traffic flow evolution with AdapKoopPC under communication range degradation

3) *CAVs distribution*: To compare the control performance of AdapKoopPC in mitigating traffic oscillations under different CAV distributions in the mixed traffic flow, the arrangements of HDVs and CAVs are randomly generated while maintaining a fixed CAV penetration rate of 10%. Fig. 14 aims to explore the impact of AdapKoopPC on alleviating traffic oscillations under different CAV distributions. Fig. 14 (a) corresponds to a scenario where three CAVs are concentrated in the front of the mixed traffic flow, and its optimization effect on the mixed traffic flow is very close to Fig. 12 (c). This is related to the fact that CAVs in the front of the mixed traffic flow can eliminate oscillations almost without affecting subsequent vehicles. Fig. 14 (b) and Fig. 14 (c) correspond to the concentration of CAVs in the middle and rear of all vehicles, respectively. It can be observed that the effect is not as good as when CAVs are located in the front, which is understandable. Yet, the overall disturbance mitigation effect

is significant. Additionally, an interesting finding is that when CAVs are more evenly distributed, the mitigation performance is better than when they are concentrated in the middle or rear. Overall, regardless of the position of the CAVs, AdapKoopPC performs well, fully demonstrating its effectiveness and universality, strong generalization ability, and suitability for various scenarios.

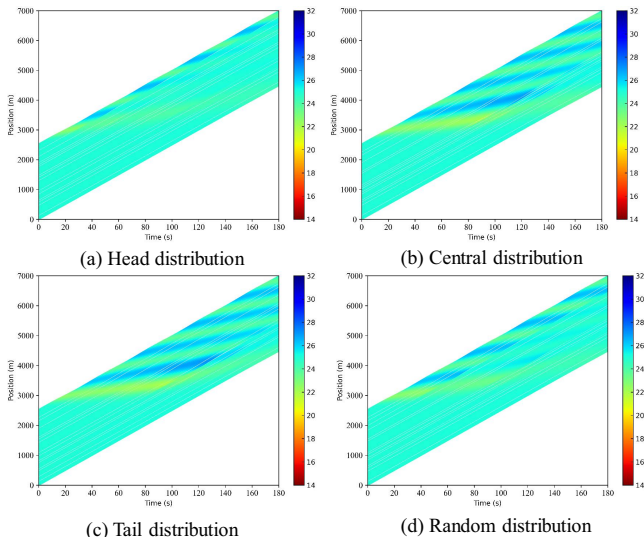


Fig. 14. The mixed traffic flow evolution with AdapKoopPC under different CAVs distribution

4) *Number of controller deployments*: We further investigate how many CAVs are required to deploy the proposed AdapKoopPC controller in random conditions to achieve a satisfactory level of traffic flow improvement. A mixed traffic flow consisting of 20 CAVs and 30 HDVs were randomly generated, where the AdapKoopPC was randomly deployed on the CAVs. In order to quantitatively analyze the traffic flow improvement, the velocity standard deviation and headway standard deviation of all vehicles in the mixed traffic flow are used as evaluation indicators. The results are shown in Table V. Overall, as the number of deployed controllers increases, the standard deviation of speed and headway gradually decreases. More importantly, the standard deviation of speed and headway archives convergence when the controller was 15 in such a mixed traffic flow. At such situation, the speed oscillation was reduced by 52.12%, and the standard deviation of the headway was reduced by 53.36%.

TABLE V  
THE IMPACT OF THE NUMBER OF CONTROLLERS ON REDUCING TRAFFIC FLOW OSCILLATIONS

Number	$v_{std}$ (m/s)	$h_{std}$ (m)	Number	$v_{std}$	$h_{std}$ (m)
0	3.30	8.34	1	2.28	5.55
2	2.18	5.47	3	2.16	5.65
4	2.07	5.48	5	2.04	5.55
6	1.85	4.85	7	1.84	4.86
8	1.65	4.15	9	1.61	3.99
10	1.61	3.98	11	1.59	3.92
12	1.60	3.94	13	1.58	3.89
14	1.58	3.88	15	1.58	3.89
16	1.59	3.86	17	1.59	3.84
18	1.59	3.83	19	1.59	3.83
20	1.59	3.81	/	/	/

## VII. CONCLUSIONS

The main challenge currently faced by optimizing mixed traffic flow through CAVs is to accurately recognize and predict the driving behavior of HDVs while meeting real-time online computing capabilities. The Koopman operator theory and extended dynamic mode decomposition can achieve the linear approximation of nonlinear dynamic systems in high-dimensional space, providing feasible solutions for current issues. In this study, we propose AdapKoopnet to realistically describe and predict the HDVs driving behavior in complex scenarios. Furthermore, the AdapKoopPC within a predictive control framework is developed to optimize real-time control of mixed traffic flow. AdapKoopnet has the capability to adaptively cluster potential driving scenarios and extract driving features from HDVs historical trajectories, which are then fused with the explicit state of the vehicle to form a high-dimensional representation of the state. The AdapKoopPC integrates AdapKoopnet and benefits from its linear characteristics, to achieve more efficient real-time control of CAVs in mixed traffic flow. Subsequently, trajectory prediction and traffic flow control optimization experiments are conducted, the following conclusions are mainly drawn:

- Benefiting from the Koopman theory, the multi-step prediction performance of AdapKoopnet based on linear space surpasses LSTM-based nonlinear encoder-decoder of the same dimension. And the semantic extraction of trajectory context plays an indispensable positive role in the accuracy of HDVs state prediction;
- With the appropriate architecture and loss function design of AdapKoopnet, it achieves powerful trajectory clustering and scenario recognition without pre-label, as well as adaptive driving characteristics extraction;
- AdapKoopPC does not rely on prior car following model or pre-collected simulation trajectories, has better scenario generalization ability. In small-scale experiments, AdapKoopPC has shown promising results in slowing down traffic disturbance oscillations and improving traffic flow stability. Compared with baseline models, it has more satisfactory computational efficiency and practical application potential;
- The large-scale experimental results show that when the penetration rate of CAVs is 20%, the inhibitory effect of AdapKoopPC on oscillations is close to saturation. Besides, in the case of communication degradation, the control effect of AdapKoopPC with 20% CAV penetration rate is roughly equivalent to that of a 10% CAV penetration rate without communication loss; Moreover, the control effect of AdapKoopPC varies under different CAVs distributions, yet consistently exhibit superior performance in all cases.

There are some limitations of this study. For example, Koopman operator does not support online updates. And AdapKoopPC still faces dimensional disasters under ultra large scale mixed traffic flow. In future work, the online learning and efficient distributed control framework will be developed. Furthermore, expanding the application scenario of AdapKoopPC to multiple lanes is also worth further exploration.



## REFERENCES

- [1] P. Bansal, D. J. Graham *et al.*, “Congestion in cities: Can road capacity expansions provide a solution?” *Transportation Research Part A: Policy and Practice*, vol. 174, p. 103726, 2023.
- [2] S. Wang, Z. Wang, R. Jiang, F. Zhu, R. Yan, and Y. Shang, “A multi-agent reinforcement learning-based longitudinal and lateral control of cavs to improve traffic efficiency in a mandatory lane change scenario,” *Transportation Research Part C: Emerging Technologies*, vol. 158, p. 104445, 2024.
- [3] L. Li, H. Lyu, T. Wang, and R. Cheng, “Std4dmpc: Distributed model predictive control for connected and automated truck platoon with mixed traffic flow based on spatiotemporal trajectory prediction,” *IEEE Transactions on Vehicular Technology*, 2024.
- [4] K. C. Dey, L. Yan, X. Wang, Y. Wang, H. Shen, M. Chowdhury, L. Yu, C. Qiu, and V. Soundararaj, “A review of communication, driver characteristics, and controls aspects of cooperative adaptive cruise control (cacc),” *IEEE Transactions on Intelligent Transportation Systems*, vol. 17, no. 2, pp. 491–509, 2015.
- [5] A. Matin and H. Dia, “Impacts of connected and automated vehicles on road safety and efficiency: A systematic literature review,” *IEEE Transactions on Intelligent Transportation Systems*, 2022.
- [6] D. Chen, H. Huang, Y. Zheng, P. Gawkowski, H. Lv, and Z. Lv, “The scanner of heterogeneous traffic flow in smart cities by an updating model of connected and automated vehicles,” *IEEE Transactions on Intelligent Transportation Systems*, vol. 23, no. 12, pp. 25 361–25 370, 2022.
- [7] Y. Du, M. A. Makridis, C. M. Tampère, A. Kouvelas, and W. Shang-Guan, “Adaptive control with moving actuators at motorway bottlenecks with connected and automated vehicles,” *Transportation Research Part C: Emerging Technologies*, vol. 156, p. 104319, 2023.
- [8] Z. Wang, Y. Bian, S. E. Shladover, G. Wu, S. E. Li, and M. J. Barth, “A survey on cooperative longitudinal motion control of multiple connected and automated vehicles,” *IEEE Intelligent Transportation Systems Magazine*, vol. 12, no. 1, pp. 4–24, 2019.
- [9] S. Cui, F. Cao, B. Yu, and B. Yao, “Modeling heterogeneous traffic mixing regular, connected, and connected-autonomous vehicles under connected environment,” *IEEE Transactions on Intelligent Transportation Systems*, vol. 23, no. 7, pp. 8579–8594, 2021.
- [10] M. Bando, K. Hasebe, K. Nakanishi, and A. Nakayama, “Analysis of optimal velocity model with explicit delay,” *Physical Review E*, vol. 58, no. 5, p. 5429, 1998.
- [11] R. Jiang, M.-B. Hu, H. Zhang, Z.-Y. Gao, B. Jia, and Q.-S. Wu, “On some experimental features of car-following behavior and how to model them,” *Transportation Research Part B: Methodological*, vol. 80, pp. 338–354, 2015.
- [12] M. Treiber, A. Hennecke, and D. Helbing, “Congested traffic states in empirical observations and microscopic simulations,” *Physical Review E*, vol. 62, no. 2, p. 1805, 2000.
- [13] S. Li, D. Yanagisawa, and K. Nishinari, “A jam-absorption driving system for reducing multiple moving jams by estimating moving jam propagation,” *Transportation Research Part C: Emerging Technologies*, vol. 158, p. 104394, 2024.
- [14] J. Wang, Y. Zheng, C. Chen, Q. Xu, and K. Li, “Leading cruise control in mixed traffic flow: System modeling, controllability, and string stability,” *IEEE Transactions on Intelligent Transportation Systems*, vol. 23, no. 8, pp. 12 861–12 876, 2021.
- [15] Y. Zheng, J. Wang, and K. Li, “Smoothing traffic flow via control of autonomous vehicles,” *IEEE Internet of Things Journal*, vol. 7, no. 5, pp. 3882–3896, 2020.
- [16] J. Wang, Y. Zheng, Q. Xu, J. Wang, and K. Li, “Controllability analysis and optimal control of mixed traffic flow with human-driven and autonomous vehicles,” *IEEE Transactions on Intelligent Transportation Systems*, vol. 22, no. 12, pp. 7445–7459, 2020.
- [17] J. Wang, Y. Zheng, K. Li, and Q. Xu, “Deep-lcc: Data-enabled predictive leading cruise control in mixed traffic flow,” *IEEE Transactions on Control Systems Technology*, 2023.
- [18] J. Wang, Y. Lian, Y. Jiang, Q. Xu, K. Li, and C. N. Jones, “Distributed data-driven predictive control for cooperatively smoothing mixed traffic flow,” *Transportation Research Part C: Emerging Technologies*, vol. 155, p. 104274, 2023.
- [19] F. Montanari, R. German, and A. Djanatliev, “Pattern recognition for driving scenario detection in real driving data,” in *2020 IEEE Intelligent Vehicles Symposium (IV)*. IEEE, 2020, pp. 590–597.
- [20] S. Jarl, L. Aronsson, S. Rahrovani, and M. H. Chehreghani, “Active learning of driving scenario trajectories,” *Engineering Applications of Artificial Intelligence*, vol. 113, p. 104972, 2022.
- [21] G. Li, Y. Chen, D. Cao, X. Qu, B. Cheng, and K. Li, “Extraction of descriptive driving patterns from driving data using unsupervised algorithms,” *Mechanical Systems and Signal Processing*, vol. 156, p. 107589, 2021.
- [22] Y. Xing, C. Lv, and D. Cao, “Personalized vehicle trajectory prediction based on joint time-series modeling for connected vehicles,” *IEEE Transactions on Vehicular Technology*, vol. 69, no. 2, pp. 1341–1352, 2019.
- [23] B. Gao, K. Cai, T. Qu, Y. Hu, and H. Chen, “Personalized adaptive cruise control based on online driving style recognition technology and model predictive control,” *IEEE Transactions on Vehicular Technology*, vol. 69, no. 11, pp. 12 482–12 496, 2020.
- [24] Y. Zhang, X. Chen, J. Wang, Z. Zheng, and K. Wu, “A generative car-following model conditioned on driving styles,” *Transportation Research Part C: Emerging Technologies*, vol. 145, p. 103926, 2022.
- [25] T. Gindele, S. Brechtel, and R. Dillmann, “A probabilistic model for estimating driver behaviors and vehicle trajectories in traffic environments,” in *13th International IEEE Conference on Intelligent Transportation Systems*. IEEE, 2010, pp. 1625–1631.
- [26] M. Zhou, X. Qu, and S. Jin, “On the impact of cooperative autonomous vehicles in improving freeway merging: a modified intelligent driver model-based approach,” *IEEE Transactions on Intelligent Transportation Systems*, vol. 18, no. 6, pp. 1422–1428, 2016.
- [27] L. Lin, W. Li, H. Bi, and L. Qin, “Vehicle trajectory prediction using lstms with spatial-temporal attention mechanisms,” *IEEE Intelligent Transportation Systems Magazine*, vol. 14, no. 2, pp. 197–208, 2021.
- [28] Z. Mo, R. Shi, and X. Di, “A physics-informed deep learning paradigm for car-following models,” *Transportation Research Part C: Emerging Technologies*, vol. 130, p. 103240, 2021.
- [29] M. Geng, J. Li, Y. Xia, and X. M. Chen, “A physics-informed transformer model for vehicle trajectory prediction on highways,” *Transportation Research Part C: Emerging Technologies*, vol. 154, p. 104272, 2023.
- [30] S. Feng, Z. Song, Z. Li, Y. Zhang, and L. Li, “Robust platoon control in mixed traffic flow based on tube model predictive control,” *IEEE Transactions on Intelligent Vehicles*, vol. 6, no. 4, pp. 711–722, 2021.
- [31] H. Shi, Y. Zhou, K. Wu, X. Wang, Y. Lin, and B. Ran, “Connected automated vehicle cooperative control with a deep reinforcement learning approach in a mixed traffic environment,” *Transportation Research Part C: Emerging Technologies*, vol. 133, p. 103421, 2021.
- [32] R. E. Stern, S. Cui, M. L. Delle Monache, R. Bhadani, M. Bunting, M. Churchill, N. Hamilton, H. Pohlmann, F. Wu, B. Piccoli *et al.*, “Dissipation of stop-and-go waves via control of autonomous vehicles: Field experiments,” *Transportation Research Part C: Emerging Technologies*, vol. 89, pp. 205–221, 2018.
- [33] Y. Wang, Y. Jiang, Y. Wu, and Z. Yao, “Mitigating traffic oscillation through control of connected automated vehicles: A cellular automata simulation,” *Expert Systems with Applications*, vol. 235, p. 121275, 2024.
- [34] K. Li, J. Wang, and Y. Zheng, “Cooperative formation of autonomous vehicles in mixed traffic flow: Beyond platooning,” *IEEE Transactions on Intelligent Transportation Systems*, vol. 23, no. 9, pp. 15 951–15 966, 2022.
- [35] N. Lichtlé, E. Vinitzky, M. Nice, B. Seibold, D. Work, and A. M. Bayen, “Deploying traffic smoothing cruise controllers learned from trajectory data,” in *2022 International Conference on Robotics and Automation (ICRA)*. IEEE, 2022, pp. 2884–2890.
- [36] X. Yue, H. Shi, Y. Zhou, and Z. Li, “Hybrid car following control for cavs: Integrating linear feedback and deep reinforcement learning to stabilize mixed traffic,” *Transportation Research Part C: Emerging Technologies*, vol. 167, p. 104773, 2024.
- [37] C. Zhao and H. Yu, “Robust safety for mixed-autonomy traffic with delays and disturbances,” *IEEE Transactions on Intelligent Transportation Systems*, 2024.
- [38] J. Zhan, Z. Ma, and L. Zhang, “Data-driven modeling and distributed predictive control of mixed vehicle platoons,” *IEEE Transactions on Intelligent Vehicles*, vol. 8, no. 1, pp. 572–582, 2022.
- [39] B. O. Koopman, “Hamiltonian systems and transformation in hilbert space,” *Proceedings of the National Academy of Sciences*, vol. 17, no. 5, pp. 315–318, 1931.
- [40] A. M. Avila and I. Mezić, “Data-driven analysis and forecasting of highway traffic dynamics,” *Nature communications*, vol. 11, no. 1, p. 2090, 2020.
- [41] E. Ling, L. Zheng, L. J. Ratliff, and S. Coogan, “Koopman operator applications in signalized traffic systems,” *IEEE Transactions on Intelligent Transportation Systems*, vol. 23, no. 4, pp. 3214–3225, 2020.

- [42] C. Gu, T. Zhou, and C. Wu, "Deep koopman traffic modeling for free-way ramp metering," *IEEE Transactions on Intelligent Transportation Systems*, 2023.
- [43] Y. Xiao, X. Zhang, X. Xu, X. Liu, and J. Liu, "Deep neural networks with koopman operators for modeling and control of autonomous vehicles," *IEEE Transactions on Intelligent Vehicles*, vol. 8, no. 1, pp. 135–146, 2022.
- [44] Y. Liu, C. Li, J. Wang, and M. Long, "Koopman: Learning non-stationary time series dynamics with koopman predictors," *arXiv preprint arXiv:2305.18803*, 2023.
- [45] J. L. Proctor, S. L. Brunton, and J. N. Kutz, "Generalizing koopman theory to allow for inputs and control," *SIAM Journal on Applied Dynamical Systems*, vol. 17, no. 1, pp. 909–930, 2018.
- [46] M. O. Williams, I. G. Kevrekidis, and C. W. Rowley, "A data-driven approximation of the koopman operator: Extending dynamic mode decomposition," *Journal of Nonlinear Science*, vol. 25, pp. 1307–1346, 2015.
- [47] A. Vaswani, N. Shazeer, N. Parmar, J. Uszkoreit, L. Jones, A. N. Gomez, L. Kaiser, and I. Polosukhin, "Attention is all you need," *Advances in Neural Information Processing Systems*, vol. 30, 2017.
- [48] J. L. Ba, J. R. Kiros, and G. E. Hinton, "Layer normalization," *arXiv preprint arXiv:1607.06450*, 2016.
- [49] B. Lusch, J. N. Kutz, and S. L. Brunton, "Deep learning for universal linear embeddings of nonlinear dynamics," *Nature communications*, vol. 9, no. 1, p. 4950, 2018.
- [50] S. Liu, E. Johns, and A. J. Davison, "End-to-end multi-task learning with attention," in *Proceedings of the IEEE/CVF Conference on Computer Vision and Pattern Recognition*, 2019, pp. 1871–1880.
- [51] S. H. Park, B. Kim, C. M. Kang, C. C. Chung, and J. W. Choi, "Sequence-to-sequence prediction of vehicle trajectory via lstm encoder-decoder architecture," in *2018 IEEE Intelligent Vehicles Symposium (IV)*. IEEE, 2018, pp. 1672–1678.
- [52] T. Ruan, H. Wang, L. Zhou, Y. Zhang, C. Dong, and Z. Zuo, "Impacts of information flow topology on traffic dynamics of cav-mv heterogeneous flow," *IEEE Transactions on Intelligent Transportation Systems*, vol. 23, no. 11, pp. 20 820–20 835, 2022.